CHALMERS
UNIVERSITY OF TECHNOLOGY

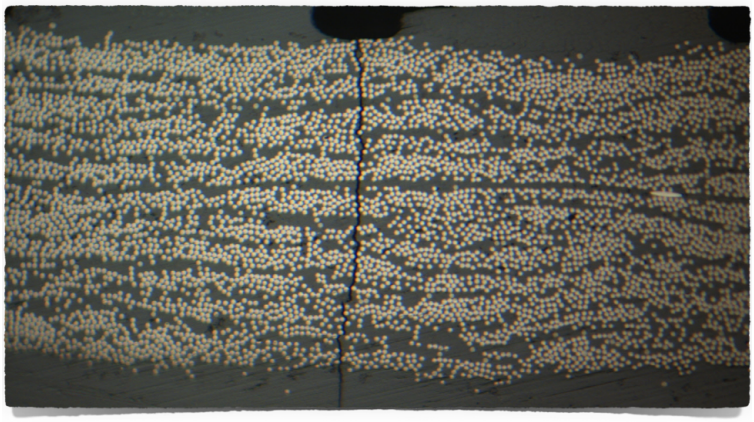

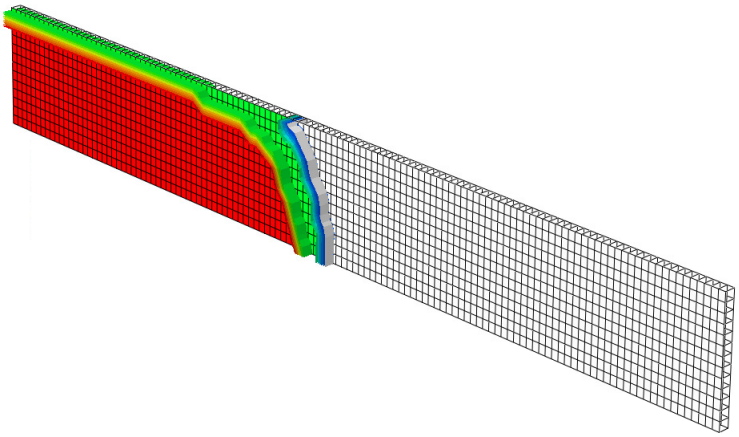

Numerical and experimental analysis of the mechanical response of thin-ply cross-ply composites

Master's thesis in Applied Mechanics

ROBIN HAGVALL
SIMON JOHANSSON

Department of Industrial and Materials Science
CHALMERS UNIVERSITY OF TECHNOLOGY
Gothenburg, Sweden 2019

Master's thesis 2019

Numerical and experimental analysis of the mechanical response of thin-ply cross-ply composites

ROBIN HAGVALL
SIMON JOHANSSON

CHALMERS
UNIVERSITY OF TECHNOLOGY

Department of Industrial and Materials Science
Division of Material and Computational Mechanics
Chalmers University of Technology
Gothenburg, Sweden 2019

Numerical and experimental analysis of the mechanical response of
thin-ply cross-ply composites
Master's thesis in Applied Mechanics
ROBIN HAGVALL, SIMON JOHANSSON

© ROBIN HAGVALL, SIMON JOHANSSON, 2019.

Supervisor: Peter Linde, Research engineer at Airbus and Adjunct Professor at the Department of Industrial and Materials Science
Examiner: Leif Asp, Professor at the Department of Industrial and Materials Science

Master's Thesis 2019
Department of Industrial and Materials Science
Division of Material and Computational Mechanics
Chalmers University of Technology
SE-412 96 Gothenburg
Telephone +46 31 772 1000

Cover: Transverse matrix crack from experimental and numerical analyses.

Typeset in LaTeX
Gothenburg, Sweden 2019

Numerical and experimental analysis of the mechanical response of thin-ply cross-ply composites
Master's thesis in Applied Mechanics
ROBIN HAGVALL
SIMON JOHANSSON
Department of Industrial and Materials Science
Chalmers University of Technology

Abstract

One of the major strivings of today is to reduce the emission of green house gases. Within the transport vehicle industry this can be achieved by reducing their structural weight, which lowers the fuel consumption. That strive motivates the use of fibre reinforced polymers, which offers an increased weight to stiffness ratio compared to metallic materials. Moreover, it has been shown that further advantages can be achieved if the thickness of certain plies in a composite is reduced. More specifically, if the thickness of a transversely loaded ply embedded in a multidirectional laminate is reduced, the onset of transverse cracks can be substantially delayed. This is called the in-situ effect.

The aim of this project is to, with one experimental study and one numerical study, investigate this in-situ effect for thinner plies for which it has not yet been fully established. The thickness range considered is between 20 µm and 240 µm. For the experimental study test specimens are manufactured and subjected to a tensile load while the edges are inspected for cracks. The numerical analysis is conducted within the framework of Abaqus, where a cohesive zone model is developed in combination with extended FEM.

The outcome of the experiments show a small delay in the onset of transverse cracks when the thickness of the 90°-ply is reduced. For some cases it is also seen that the crack density decreases when the thickness is reduced. Finally, the stiffness of the adjacent plies does not seem to have a large impact on the in-situ effect. However, difficulties related to manufacturing complicates the interpretation of those results and their validity can be questioned.

The numerical study shows an in-situ effect in a model in which no in-situ properties are used. For the thinner case, the result aligns well with analytical models. It is shown that an extremely fine mesh is necessary in order to resolve the crack zone correctly, and the dependency of input variables such as the critical energy release rate and interface strength is demonstrated. It is also shown that for one of the studied material a transition from stable to unstable crack growth occurs at the thickness 80 µm, where a crack grows stably for thinner plies and unstably for a thicker plies.

Taking into account the manufacturing complications, the results still, on the whole, indicate that the in-situ effect exist for the thin-ply composites studied in this project. This further motivates the development and research connected to thin-ply composites.

Keywords: composites, cross-ply, thin-ply, in-situ, transverse cracks, extended FEM, cohesive zone modelling, applied mechanics.

Acknowledgements

We would first like to thank our supervisors Leif Asp, Professor at the department of Industrial and Materials Science, and Peter Linde, Adjunct Professor at the department of Industrial and Materials Science and research engineer in the area of aircraft integration and architecture at Airbus. Both have, with their profound knowledge and experience, been invaluable for this project.

Secondly, we would also like to thank people from the industry that have helped by supplying material, equipment and expertise. Florence Rinn and Fredrik Ohlsson at Oxeon AB, Mohamed Loukil and Peter Hellström at RISE, Per Hallander at SAAB and Lisa Müller at CTC. Their contributions were a necessity for the study to proceed.

Lastly, we would like to thank Chalmers employees Postdoc Hana Zrida, Associate Professor Martin Fagerström and Ph.D Dennis Wilhelmsson. They have all made this project possible with their specific areas of expertise.

Robin Hagvall & Simon Johansson, Gothenburg, June 2019

Nomenclature and abbreviations

σ	Stress	[Pa]
ε	Strain	[−]
E	Young's modulus	[Pa]
E_f	Young's modulus of fibre	[Pa]
E_m	Young's modulus of matrix	[Pa]
E_L	Young's modulus in longitudinal direction	[Pa]
E_T	Young's modulus in transverse direction	[Pa]
G	Energy release rate	[J/m^2]
G_{Ic}	Critical energy release rate in Mode I	[J/m^2]
Y^T	Transverse tensile strength	[Pa]
Y^T_{is}	Transverse tensile in-situ strength	[Pa]
δ	Separation	[m]
τ^0	Interface strength	[Pa]
V_f	Fibre volume fraction	[−]
ρ_f	Fibre density	[kg/m^3]
ρ_m	Matrix density	[kg/m^3]
W_f	Fibre weight	[kg]
W_m	Matrix weight	[kg]

FEM	Finite element method
XFEM	Extended finite element method
CZM	Cohesive zone modelling
LEFM	Linear elastic fracture mechanics
CLT	Classical laminate theory
FRP	Fibre reinforced polymer
CFRP	Carbon fibre reinforced polymer
GFRP	Glass fibre reinforced polymer
C20-240	Laminates purely with carbon fibres and inner-ply thickness between 20 and 240 µm
G20-240	Laminates with adjacent plies in glass fibres and inner-ply thickness between 20 and 240 µm

Contents

List of Figures

List of Tables

1

Introduction

This chapter presents a background to the subject that is studied in this Master's thesis project, including a motivation to its necessity and how it was initiated. This is followed by a description of the purpose and objectives of the study. Finally, boundaries to the scope of the study are stated.

1.1 Background

One step towards reducing the emission of green house gases caused by transport vehicles is to reduce their structural weight. This also results in cost savings due to the lower fuel consumption. That strive has motivated the use of fibre reinforced polymers (FRP), which offers a significant increase in the stiffness to weight ratio compared to metallic materials such as steel or aluminium. Moreover, composites offer other advantages e.g. vibration reduction and energy absorption. It also allows tailoring each component to meet its requirement by choosing the individual constituents and orientation of the fibre reinforcement [1].

It has been shown that further advantages can be achieved if the thickness of the FRP ply is reduced, where a higher strength can be obtained for certain configurations. More specifically, in a laminate containing plies with fibre orientations perpendicular to the loading direction the onset of transverse matrix cracks can be substantially delayed. This is called the *in-situ* effect and it has been studied thoroughly for thicknesses down to the conventional 0.1 mm. However, recently a methodology has been developed to obtain even thinner composites, down to 0.02 mm, for which the in-situ effect has not yet been fully established. It is therefore of interest to study this further.

Finite element analysis (FEA) plays an important role in studying the behaviour of structures, but also in reducing costs related to large amount of physical tests. This also holds for composite structures, however, numerical analysis of in-situ effect is still on a research stage and needs additional investigations.

To contribute data within these subjects, experimental and finite element analyses are to be conducted. The goal with the experiments is to expand the thickness range to also comprise smaller thicknesses for which the in-situ effect is studied. The goal with the FE model is to accurately predict the experimental results and to extract data that may

contribute to a deeper understanding of the underlying physical phenomena that govern the observed behaviour.

This project was initiated from a recently started collaboration between Chalmers University of Technology and the aircraft manufacturer Airbus. Parts of the work took place at Airbus facilities in Hamburg.

1.2 Purpose

The purpose of this project is to expand the current knowledge of the mechanical response of thin-ply carbon fibre reinforced polymer cross-ply laminates, i.e. show by experimental tests how reduced ply thickness increases the strain to onset of matrix cracking in the 90°-ply in a cross-ply laminate. FE analysis is to be conducted for the same configurations, and predictions are to be compared to results from mechanical testing for validation.

1.3 Objectives

The main objective of this study is to establish a reliable trend of the influence of ply thickness of the embedded 90°-ply in a cross-ply laminate on the transverse strength. The objective can be divided into the subgoals listed below.

- Manufacture a sufficient number of thin-ply composite laminates from carbon fibre reinforced polymer (CFRP) with embedded 90°-plies. To establish a reliable trend for the influence of reduced ply thickness, the thickness of the 90°-ply will vary between 0.02 mm and 0.24 mm.

- Manufacture similar laminates, but with glass fibre reinforced polymer (GFRP) in the outer plies (0°) to investigate if there is a stiffness dependency to the in-situ effect.

- Perform tensile tests on test specimens extracted from the manufactured laminates. During tensile loading the onset of transverse cracking and crack density for different strain levels in the 90° ply will be measured.

- Investigate whether cracks close when the specimen is unloaded, and in that case find a technique which allows for measurements during tensile loading.

- Investigate if cracks found on the specimen edges run through the entire lamina width or not.

- Perform finite element analysis mimicking the mechanical tests, using the commercial software Abaqus. The FE model will provide numerical results on the onset of transverse cracks for the same laminate configurations used in the experimental analysis. It is also to give information about the stability of the crack propagation.

- Compare all results with existing analytical models that are said to predict in-situ strength.

1.4 Boundaries

The different aspects of this subject are countless and cannot all be in the scope of this study. Here follows a presentation of the delimitation to what will be considered.

- More than one iteration of manufacturing does not take place due to the large time consumption related to it. Hence, potentially undesirable quality from the manufacturing is analysed and taken into account to the result.

- Tensile load is the only load case considered for both experimental and numerical analysis.

- Final failure of the laminate is not considered, nor is the progressively developing stiffness reduction that is caused by increasing crack density.

- Concerning the FEA, no other models offered by other actors than Abaqus are considered. Hence it is limited to the possibilities offered by Abaqus and existing plug-ins.

- Development of analytical models to predict in-situ strength are not within the scope of this thesis. Existing models are only used to compare experimental and FE results, without modification.

2

Literature Review

In this chapter, subjects relevant for this study are introduced and described. The goal is to present an overview of what has been done to date in terms of experimental and FE analysis of thin-ply composites and their properties when embedded in a multidirectional laminate. The literature review further motivates the need of this study and shows which knowledge gaps it aims to fill.

2.1 Matrix cracking and in-situ effect

In a laminate containing embedded plies with fibre orientations perpendicular to the loading direction, matrix cracks will develop that impair the mechanical properties of the laminate and trigger other damage modes [2]. The tensile and shear strength of the embedded plies has shown to increase compared to a unidirectional laminate, and increase further when decreasing the ply thickness [3, 4, 5, 6, 7, 8]. The crack density has also been shown to decrease with decreased ply thickness [9]. The reason is a constraining effect introduced by the neighbouring plies that limits the available elastic energy within the transverse ply, delaying the damage propagation in the matrix [10, 11]. The strengths are also affected by the stiffness and fibre orientation of the adjacent plies [12, 13, 14]. These constraint effects that determine the strengths of an embedded ply loaded transversely, are called *in-situ* effects.

Already in 1977-1978 experiments were conducted by Parvizi & Bailey [4] and Garrett & Bailey [3], on glass fibre reinforced polymer cross-ply laminates, to study the in-situ effect and its dependency on the inner-ply thickness. The result they obtained is shown in Figure 2.1a. In Figure 2.1b same in-situ effect is plotted for different carbon fibre reinforced cross-ply composites, from experimental studies by Berglund et al. [6] in 1991. More recently, in 2019, García et al. [8] carried out an extensive test campaign on cross-ply laminates of AS4/8558 carbon/epoxy, studying a wider range of thicknesses, see Figure 2.2. Once again confirming the thickness dependency of the in-situ effect.

In 1982, Flaggs and Kural [12] studied the dependency of the fibre orientation of the adjacent plies for T300/934 carbon/epoxy and found the relation illustrated in Figure 2.3. The same tendency is seen for all layups considering the thickness dependency, however, the difference between them increases as the inner-ply thickness decreases. Dvorak and Laws [14] compared experiments in 1987, carried out earlier by Crossman & Wang [13]

and Wang [15] on the same material, and found similar effects as shown in Figure 2.3. This effect is caused by the reduced stiffness obtained when increasing the angle in the adjacent plies [16].

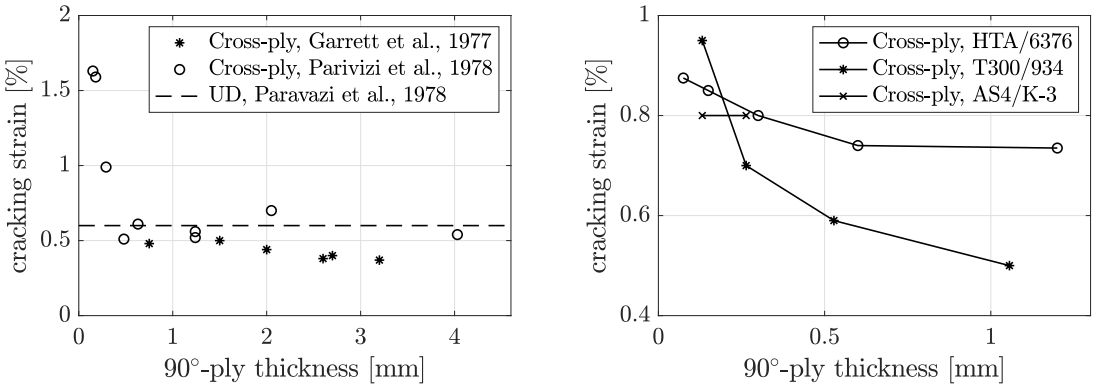

(a) GFRP **(b)** CFRP

Figure 2.1: Cracking strain for GFRP cross-ply laminates [4, 3] and CFRP cross-ply laminates [6] for different inner-ply thickness.

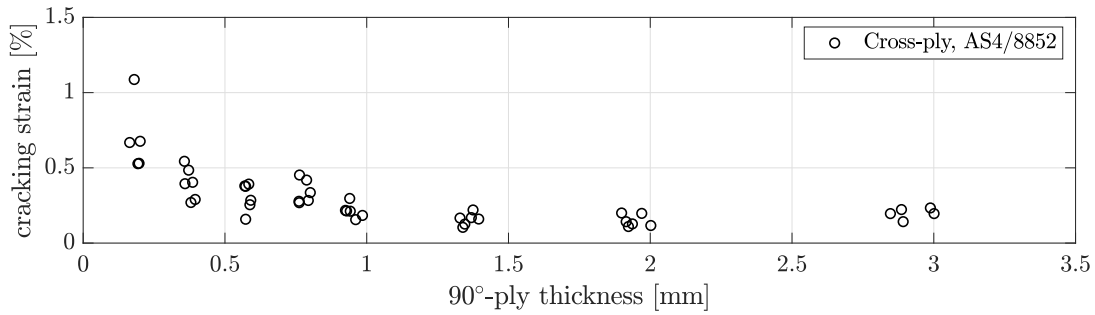

Figure 2.2: Cracking strain for AS4/8852 carbon/epoxy cross-ply laminates for different inner-ply thickness [8].

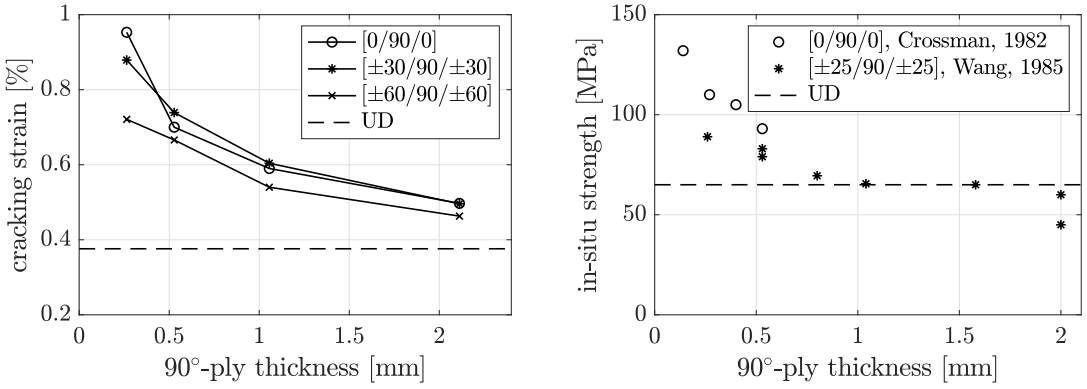

Figure 2.3: Cracking strain [12] and in-situ strength [14] for T300/9324 carbon/epoxy cross-ply laminates with different outer-ply fibre orientations.

2.2 Spread-tow thin-ply composites

The method used to achieve ultra-thin composites is called tow-spreading technology. It allows a conventional carbon fibre tow to be thinned by increasing the width from 5 mm to 25 mm [17]. The areal weight can therefore be reduced by 500 % down to around 20 g/m^2 depending on manufacturer. The present technique for tow-spreading, according to Shin et al. [18], is shown in Figure 2.4. With the help of an airflow, a pressure difference is created that arise from larger velocities at the sides of the filament. This pressure difference gives rise to a force that drives the spreading of the fibres.

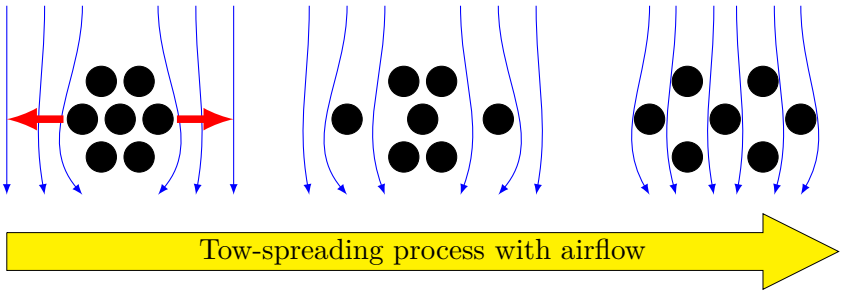

Figure 2.4: Principle sketch of tow-spreading procedure based on pressure difference from Shin et al. [18].

This technique allows the possibility to produce more lightweight and thin structures. Additionally, for a given thickness, more plies can be be used giving the opportunity to reduce the relative ply angles, which reduces interlaminar stresses and the risk for delamination [19].

Thin-ply composites are affected by the *size effect*. The size effect states that some material properties depend on the specimen size. In composites, which are relatively brittle, the strength is heavily dependent on defects since these initiate cracks. Probabilistically defects of a critical size are less likely to exist in a smaller volume - resulting in a higher strength [20, 21].

When using spread tows in fabrics, a smoother surface with smaller fibre waviness can be obtained than conventional fabrics. Therefore, they have a better surface finish and smaller crimp angles.

Finally, given the strong relationship between ply thickness and ply transverse tensile strength for embedded plies, the in-situ effect is expected to be very beneficial when using ultra-thin plies. However, as discussed in the previous section, most studies have not gone below the conventional 0.120 mm ply thickness. Amascher et al. [22] looked at laminates with ~ 0.03 mm ply thickness with layup $[45_m/90_m/-45_m/0_m]_{ns}$ and found that damage initiations in the transverse plies did not occur prior to failure of 0° plies. Arterio [23] studied woven composites with ultra-thin plies. However, the properties of simple cross-ply laminates using ultra-thin plies are yet to be established.

2.3 Analytical models of in-situ transverse strength in uniaxial tension

In a cross-ply laminate, the in-situ transverse strength can be predicted analytically by the use of fracture mechanics. In 1987, Dvorak and Laws [14] derived expressions for the energy release rates associated with the growth of a crack nucleus in the embedded 90°-ply. The width of the crack nucleus is $2\delta_0$ along the thickness, t_{90}, of the embedded 90°-ply. Furthermore, the crack can grow either in the longitudinal direction (through the width), in the transverse direction (through the thickness) or in both. The energy release rate in pure uniaxial loading is

$$G_I(T) = \frac{\pi\delta_0}{2}\Lambda_{22}^0\sigma_{22}^2 \tag{2.1}$$

for the crack growth in transverse direction and

$$G_I(L) = \frac{\pi\delta_0}{4}\Lambda_{22}^0\sigma_{22}^2 \tag{2.2}$$

for the crack growth in longitudinal direction where

$$\Lambda_{22}^0 = 2\left(\frac{1}{E_{22}} - \frac{\nu_{12}^2}{E_{11}}\right). \tag{2.3}$$

Since the energy release rate in the transverse direction is twice as large as in the longitudinal direction the crack will grow in the transverse direction. For the fracture energy, G_{Ic}, and the critical crack length, δ_c, and Equation (2.1) gives the in-situ transverse tensile strength Y_{is}^T as

$$Y_{is}^T = \sqrt{\frac{2G_{Ic}(T)}{\pi\delta_c(T)\Lambda_{22}^0}}. \tag{2.4}$$

Equation (2.4) is valid for thick embedded plies since $\delta_c/t_{90} \ll 1$. Due to the fact that δ_c is an unknown material characteristic Dvorak and Laws [14] proposed

$$Y_{is}^T = 1.12\sqrt{2}Y^T \tag{2.5}$$

instead to relate the thick ply transverse in-situ tensile strength with tensile strength, Y^T, for a unidirectional laminate. From Equations (2.4) and (2.5) the stress intensity magnification 1.12 along with the fracture toughness

$$G_{Ic}(T) = 1.12^2\pi\delta_c\Lambda_{22}^0(Y^T)^2 \tag{2.6}$$

has been derived. This holds since the unidirectional laminate can be considered as a special case of a thick constrained 90° ply [24].

For thin embedded plies the crack will extend over the thickness and is restricted to grow in the longitudinal direction. Hence, with $t_{90} = 2\delta_c$, Equation (2.2) gives the in-situ transverse tensile strength

$$Y_{is}^{T} = \sqrt{\frac{8G_{Ic}(L)}{\pi t_{90}\Lambda_{22}^{0}}}. \tag{2.7}$$

In Figure 2.5 the theoretical results from Equations (2.5) and (2.7) are compared to experimental results of T300/934 CFRP with $G_{Ic} = 220\,\mathrm{J/m^2}$ [14].

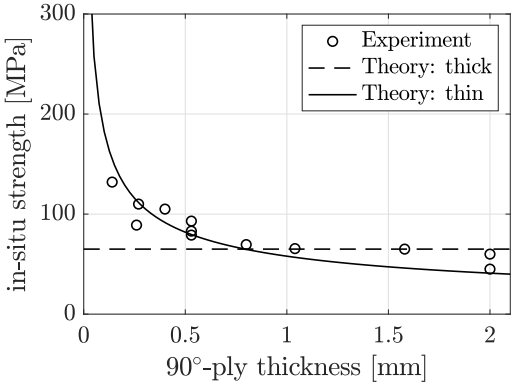

Figure 2.5: Comparison of analytical model with experimental data of T300/934 CFRP for $G_{Ic} = 220\,\mathrm{J/m^2}$ [14].

2.4 Finite element modelling of damage in composites

Modelling of composites can be done on different scales: micro-, meso- and macro-mechanical, as illustrated in Figure 2.6. In this section the basic principles of the three approaches are discussed with focus on the ability to predict the damage progression and potentially the in-situ effect.

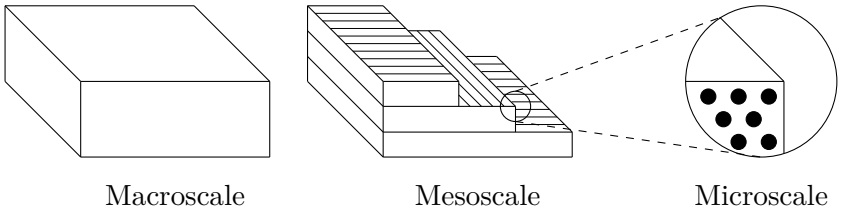

Figure 2.6: The three different approaches of FE modelling a composite: macroscale, mesoscale and microscale.

In a micro-mechanical model each constituent is modelled [25]. The fibres, the matrix and the interface between them, with their individual properties, are discretised separately. If statistically representative arrangement of the reinforcement can be established, all damage mechanisms can be modelled and generalised into a representative volume element (RVE) [26]. Both generating the RVE (randomly or with analysis of cross-sections of real composites) and FE solution is very time consuming and computationally heavy. Arteiro et al. [26] were able to predict the in-situ effect with such a model that agree with the

analytical models developed by Camanho et al. [24], however, emphasising the very fine discretisation needed and its unsuitability for larger composite structures.

On macroscale the composite is modelled with same material homogenised through the thickness. Damage progression such a delamination and microcracks can therefore not be obtained, limiting its applicability [25].

It is therefore of interest to use a meso-mechanical model. Such a model requires less computational effort than a micro-mechanical model as the discretisation is made ply-by-ply and have the capability to capture damage progression which a macro-mechanical model does not. In such a model orthotropic material properties are defined on a lamina scale, obtained from experiments or homogenised from a micro-mechanical model [26].

2.4.1 Different approaches to meso-mechanical modelling

There are different approaches to assess damage progression with a meso-mechanical model. Here continuum damage mechanics (CDM), cohesive zone modelling (CZM) and extended FEM (XFEM) are briefly discussed.

CDM is a method that relates stress to strain via some potential (e.g. the complementary free energy) that is a function of damage variables [27]. The initiation of damage is defined by a separate criterion (e.g Hashin, maximum stress or Tsai Hill). Such a model allows progressive damage within an element as well as throughout mesh. However, the in-situ strengths must be given as an input to the selected failure criterion [27].

In CZM an interface is modelled with a degradation function (e.g. a traction-separation law) where the traction between two surfaces degrades as the separation increases between them. This is usually used to model delamination [28] between plies, but can also be used to model crack propagation with the traction between the crack surfaces as the material degrades. Van der Meer et al. [29] recently performed a study with this method in combination with XFEM, which is described below.

The XFEM approach, originating from the work done by Belytachko and Black [30] and Moës et al. [31]. This method deals with the difficulty of allowing a crack to propagate in a mesh - which modifies the mesh topology. It would be necessary to re-mesh for each step, however, XFEM adds discontinuous enrichment functions to the finite element approximation [32]. Therefore discontinuities can run through elements making possible the introduction of cracks independently of mesh orientation [33]. Van der Meer et al. [29] developed a 3D model, that for a simple cross-ply laminate, was able to capture the in-situ strength using cohesive XFEM cracks. Their results are shown in Figure 2.7, where the experimental data plotted is from experiments by Crossman [13] and Wang [15]. It can be seen that for the analytical model the $G_{Ic} = 220\,\mathrm{J/m^2}$ gave the best match, while for the simulation $G_{Ic} = 170\,\mathrm{J/m^2}$ gave the best match. It was also possible to predict crack density when a statistical variation of the properties had been applied.

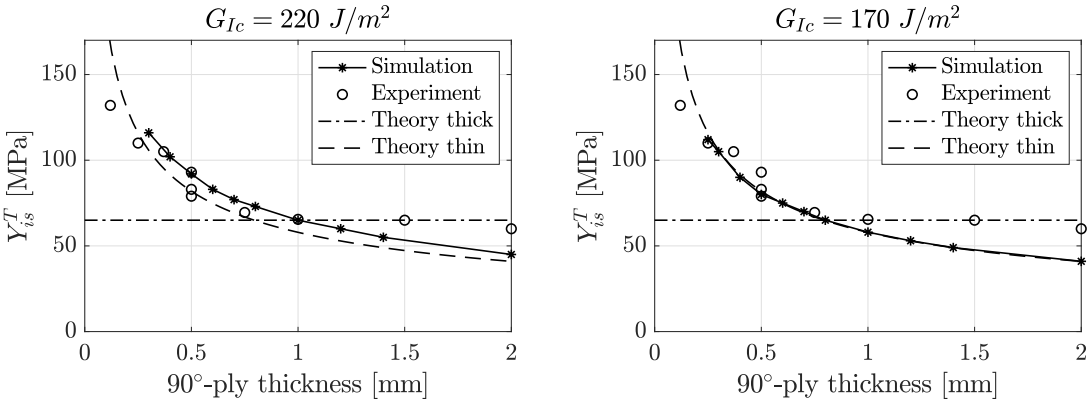

Figure 2.7: Results from a CZM model in combination with XFEM model by Van der Meer [29].

3

Theory

In this chapter, relevant theory of concepts and methods used and are crucial in order to fully understand the following chapters are presented.

3.1 Failure modes in fibre reinforced composites

In tensile loading, due to the inhomogeneous properties of fibre reinforced composites, the material experience several failure modes prior to the final failure of the structure. Damage usually initiate at defects in the material, which can be weak interfacial bonding between matrix and fibres or voids in the matrix. Thereafter, damage evolution can generally be divided into three damage modes: matrix cracking, delamination and finally fibre breakage [34]. These failure modes are schematically depicted in Figure 3.1.

Matrix cracking is usually the first mode of damage. Since the strength and stiffness properties are relatively low in the transverse direction of a ply, transverse matrix cracks or intralaminar cracks will develop parallel to the fibres. This damage mode significantly reduces the effective properties of the composite. When the matrix crack reaches the ply interface delamination cracks are induced causing the plies to separate. As a result, the stiffness degrades with a risk for catastrophic failure. Fibre breakage is the ultimately failure of the composite structure. For a unidirectional laminate loaded in longitudinal direction, fibres will break at their weakest point. The loading capacity of the laminate will decrease for each fibre breakage and the stress redistribution will affect fibres in the vicinity of the broken ones [34].

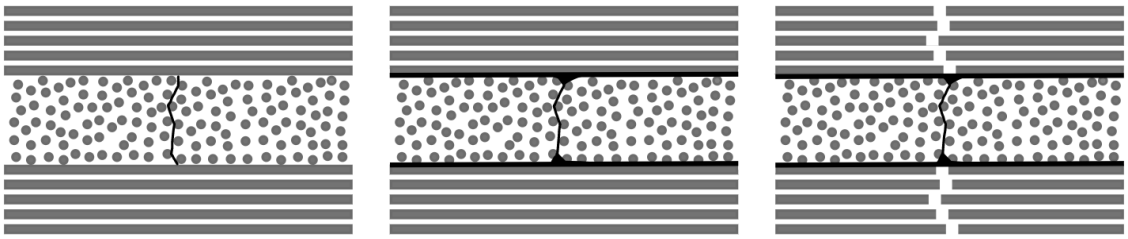

Figure 3.1: Schematic figure of matrix cracking, delamination and fibre breakage.

3.2 Extended FEM

Extended FEM (XFEM) is a method that allows modelling of cracks independently of mesh. Hence, initiation and propagation of cracks can be simulated without the need for re-meshing. The basic XFEM concept is to allow discontinuities in elements by enriching the degrees of freedom with a special displacement function. The displacement vector is now instead given as

$$\mathbf{u} = \sum_{i=1}^{N} \mathbf{N}_i(\mathbf{x}) \left[\mathbf{a}_i + \mathbf{H}_i(\mathbf{x})\mathbf{b}_i + \sum_{j=1}^{4} \mathbf{F}_j(\mathbf{x})\mathbf{c}_{i,j} \right], \tag{3.1}$$

where the shape functions $\mathbf{N}_i$ and nodal displacement vector $\mathbf{a}$ applies to all the nodes in the model. The jump function $\mathbf{H}_i$ and nodal enriched degree of freedom vector $\mathbf{b}$ applies to nodes whose shape function support is cut by the crack interior. Finally the asymptotic crack-tip functions $\mathbf{F}_i^{\alpha}$ and nodal enriched degree of freedom vector $\mathbf{c}^{\alpha}$ applies to the nodes whose shape function support is cut by the crack tip. In Figure 3.2 the areas for each part of the enrichment function can be seen, where the colours correspond to the colours in Equation (3.1). For a stationary crack the full enrichment is considered, however, for a propagating crack the last term can be excluded. This means that the crack has to propagate through the whole element at once not needing to model the stress singularity.

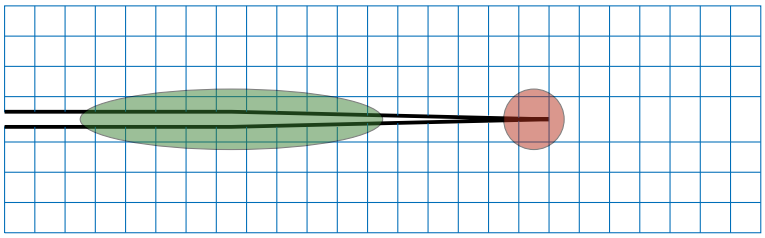

Figure 3.2: The different areas within mesh using XFEM, where each colour correspond to the enrichment presented in Equation (3.1).

Within the framework of XFEM, there are a few damage models that can be used. There is the linear elastic fracture mechanics approach (LEFM) and there is cohesive zone modelling (CZM). The latter one is used in this study and the basic concept of it is presented below.

3.3 Cohesive zone modelling

In a CZM model, phantom nodes are introduced at the defined crack surfaces. Between those nodes a traction τ is applied depending on the distance δ between them. The behaviour is described with a traction-separation law that can have arbitrary shape, one example of a bi-linear shown to the left in Figure 3.3. The damage initiation is defined in terms of a maximum/principal stress or strain until which the surfaces act linearly elastic. When the damage initiation criteria is fulfilled, denoted by interface strength τ^0

and separation δ^0, degradation begins to develop until no traction is left between the surfaces at separation δ^f. The softening constitutive behaviour is defined as [35]

$$\tau = \begin{cases} K\delta & \text{if } \delta^{max} \leq \delta^0 \\ (1-D)K\delta & \text{if } \delta^0 < \delta^{max} < \delta^f \\ 0 & \text{if } \delta^{max} \geq \delta^f \end{cases} \tag{3.2}$$

where K is the tangent stiffness matrix, δ^{max} is the maximum relative displacement and D is the scalar damage variable

$$D = \frac{\delta^f(\delta^{max} - \delta^0)}{\delta^{max}(\delta^f - \delta^0)}, \qquad D \in [0, 1]. \tag{3.3}$$

The zone in which degradation has started to develop is usually called the cohesive zone, l_{cz}, and a principle sketch of to elements in that zone is shown to the right in the figure. The area below the curve in the traction-separation law is equivalent to the critical energy release rate, G_{Ic}, i.e. the energy release rate that has to be reached for the crack to propagate.

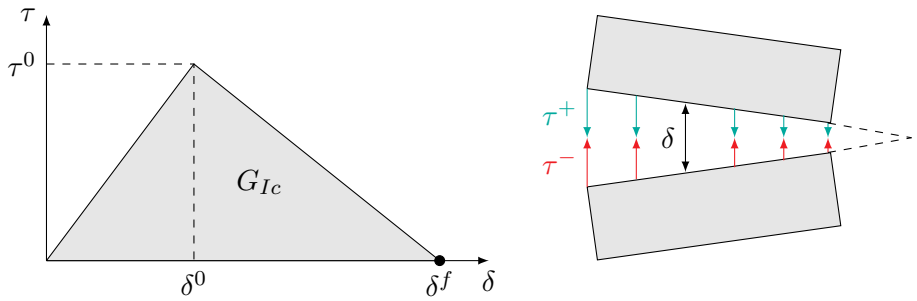

Figure 3.3: Example of a bi-linear traction-separation law in pure Mode I to the left and a principle sketch of two elements in the cohesive zone near a crack tip.

The upsides with a CZM model is that it can predict both onset and propagation of damage, without the need to remesh. On the other hand, it is associated with numerical complications regarding the definition of stiffness between the cohesive layers and the need for an extremely fine mesh [36]. If a cohesive zone have a too coarse mesh, the traction cannot be represented accurately in front of the crack tip. However, there is no consistency in the guidelines to how many elements to be used over the length of the cohesive zone, as some authors suggest 2-5 elements while others recommend using at least 10. Furthermore, the defined interface strength τ^0 has an influence on element size. A higher value yields a smaller cohesive zone length, shown in Figure 3.4, as the area below the curve must correspond to the critical energy release rate. Therefore, a higher interface strength must be compensated with a finer mesh if the same number of elements is to be used in l_{cz} for the two cases.

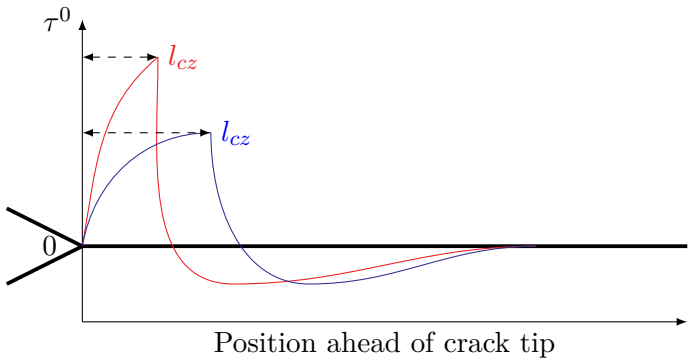

Figure 3.4: Principal sketch of cohesive zone length, l_{cz}, for different interface strength, τ^0.

4

Methodology

In this chapter the methods for all parts of the study are presented. It consists of one section describing the procedure of the experimental analysis and one section describing the finite element analysis of a matrix crack in Abaqus.

4.1 Experimental analysis

The objective of the experimental analysis is to obtain a relation between onset of a transverse crack and inner-ply thickness in a laminate where a 90°-ply is embedded in 0°-plies, i.e. the thickness dependency on in-situ effect. Furthermore, the crack density in the inner-ply for different strain levels is sought for. This is found by producing test specimens from FRP and subject them to a tensile load while the edges are studied for cracks. Both carbon and glass fibres are used for the outer-plies while the inner-plies remain from carbon. This gives information about the dependency of the stiffness. The use of glass fibres may also enable tracking propagation of individual cracks due to its transparency. Hence, two different categories of specimens are produced and tested: one only with carbon fibres and one with inner-ply from carbon fibres and outer from glass fibres. Each category contains a 90°-ply thickness that varies from 20 µm to 240 µm.

Firstly in this section the materials, layups and dimensions of the specimens are described. It is followed by a description of the manufacturing procedure and treatment of the test specimen. Finally the test procedure and measurement techniques are presented.

4.1.1 Materials

Two different materials are used throughout the manufacturing: one carbon fibre/epoxy composite and one glass fibre/epoxy composite. These are presented in more detail below.

Oxeon AB in Borås produces spread-tow unidirectional tapes called TT5082 that consists of carbon fibres MR70 and epoxy based reactive binder BI018. The tapes are 20 mm wide and 20 µm thick with the reactive binder semi cured and applied on one side of the tape. The resin content (%RC) of the composite is 38 %. The binder has been developed by Oxeon to allow pre-impregnation of ultra-light reinforcements with low %RC which could not be achieved with traditional hot melting pre-impregnating processes. BI018

Table 4.1: Properties for carbon fibre MR70 12k [37] and glass fibre E-glass.

Fibre properties	MR70 12k	E-glass[a]
Tensile modulus	324 GPa	72-85 GPa
Tensile strength	7000 MPa	1950-2050 MPa
Filament density	1.82 g/cm^3	2.55-2.6 g/cm^3
Elongation	2.16 %	2.4-2.7 %
Filament count	12k (12,000)	-
Filament diameter	5 µm	25 µm

[a] Estimated values based on similar materials.

is an epoxy resin system based on bisphenol-A, with minimum 150 °C cure temperature. However, its properties are not yet fully established.

The glass fibre used is an epoxy based pre-impregnated E-glass in a 0°/90° 4H-satin weave. This fabric has an areal weight of 107 g/m^2 and thickness 0.1 mm. The resin content is 59 %, and it cures at 180 °C. In Table 4.1 the fibre properties for both MR70 and E-glass are shown [37].

4.1.2 Layups and dimensions

All the desired layups are shown in Table 4.2 with information about the thickness, number of plies and an identification name. The identification name consists of a letter that denotes whether the 0°-plies consist of carbon (C) or glass fibres (G), and a number the denote the 90°-ply thicknesses found within the laminate. As can be seen thicknesses 20 µm, 40 µm, 80 µm, 120 µm and 240 µm are considered, where the thickest one gives comparability to earlier studies and the thinnest ones may expand the thickness range for which the in-situ effect is studied. The different thicknesses are obtained by blocking the 20 µm thick tape presented earlier in numbers of 1, 2, 4, 6 and 12. The layups C40/80 and C20/120 may seem unnecessarily complicated, however, to have the different 90°-ply thicknesses within the same laminate reduces the extent of the manufacturing and testing to be done further on as multiple thicknesses can be studied simultaneously. Note also that those two layups are identical but rotated 90°. Therefore, all the specimens with thicknesses 20 µm to 120 µm can be obtained from one laminate cut in different directions. Concerning the

Table 4.2: Layups considered to obtain desired 90°-ply thicknesses.

ID	Category	Layup	t[mm]	n_{90}	n_0
C40/80	carbon	$[0_2/90_4/0/90_2/0_3]_s$	0.48	12	12
C20/120	carbon	$[90_2/0_4/90/0_2/90_3]_s$	0.48	12	12
C240	carbon	$[0_6/90_6]_s$	0.48	12	12
G20	glass	$[0_5/90/0_5]$	1.02	1	10
G40	glass	$[0_5/90_2/0_5]$	1.04	2	10
G80	glass	$[0_5/90_4/0_5]$	1.08	4	10
G120	glass	$[0_5/90_6/0_5]$	1.12	6	10
G240	glass	$[0_5/90_{12}/0_5]$	1.24	12	10

layups that contain glass fibres, multiple thicknesses cannot be integrated within the same specimen since that would take away the possibility to, due to the transparency of the glass, see crack propagation in a single 90°-layer.

To ensure a representative sample set where each test specimen is of high quality, the dimensions and tolerances are regulated by the guidelines of the ASTM standard D3039 "Standard Test Method for Tensile Properties of Polymer Matrix Composite Materials" [38]. The geometry requirements are shown in Table 4.3. These requirements are insufficient to establish the length and width of the specimen. However, by the use of recommendations provided by ASTM 3039 [38] the length of the specimen is set to 180 mm and the width to 16 mm. The dimensions of the test specimen are shown in Figure 4.1 where the length is divided into three different regions. At the ends, grip sections are dedicated for the tensile test machine to clamp the specimen. Due to the pressure, edge effects may arise from the grips and interfere with the test results. To avoid edge effects, the middle part of the specimen where measurements will be conducted is therefore placed a distance of 20 mm from the grip section. For each of the layups presented in Table 4.2 five test specimens are manufactured with the dimensions described here.

Table 4.3: Specimen geometry requirements according to ASTM D3039 [38].

Specimen dimension	**Requirement**
length, L	$L \geq L_{grip} + 2W + L_{gauge}$
width, W	$\pm 1\,\%^a$
thickness, t	$\pm 4\,\%^a$

[a] Shall be measured at three places in the gauge section

Given the layups in Table 4.2, the longitudinal and transverse moduli can be estimated. All the C-specimen have the same moduli, and assuming a tensile modulus for the epoxy, E_m to 3 GPa and a 50 % fibre volume fraction gives, according to the rule of mixture, the longitudinal modulus

$$E_L = E_f \cdot V_f + E_m \cdot (1 - V_f) = 164\,\text{GPa} \tag{4.1}$$

and, according to Halpin-Tsai, the transverse modulus

$$E_T = E_m \frac{1 + \eta \cdot \xi \cdot V_f}{1 - \eta \cdot V_f} = 11.5\,\text{GPa}, \quad \text{with } \eta = \frac{(E_f/E_m) - 1}{(E_f/E_m) + \xi},\ \xi = 2. \tag{4.2}$$

Since the there is equal amount of 90°- and 0°-plies, the elastic modulus of the laminate is the mean of E_L and E_T, which is approximately 100 GPa. The same assumptions for

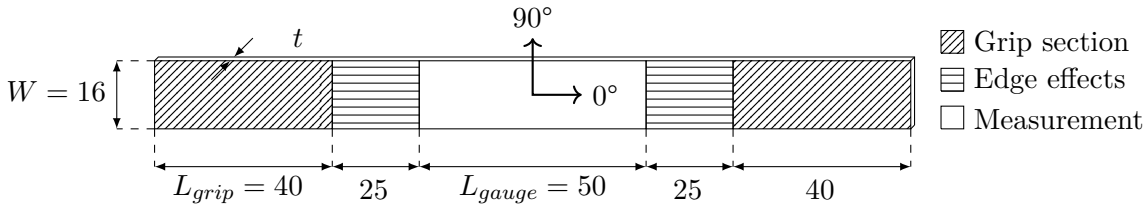

Figure 4.1: Dimensions of a test specimen in [mm].

the G-specimen gives around 35 GPa, varying a few percent depending on the thickness of the inner-ply.

4.1.3 Manufacturing

The fist step to obtain test specimens is to manufacture larger laminated plates with the desired layups, from which specimens can be cut. This is done by cutting pieces of the carbon fibre tape, peeling off the protective film and placing the tape in the desired direction one by one, side by side on a release film. Each new layer is placed on top of the former with the sticky resin rich side in the same direction, in order to obtain an even resin distribution. For every sixth ply, the laminate is vacuum bagged to remove air that may cause voids later on. For the G-specimens, that contains glass fibres, every layup is produced in one plate by placing five sheets of the woven glass fibre fabric, adding different number of blocked carbon fibre tapes on top of it and finally placing another five sheets of glass fibre. The plates are large enough so that at least five specimen can be cut out for each layup. Note that for C40/80 and C20/120 only one sheet is needed since the layups are equivalent but rotated 90°.

When the laminates are stacked they are put on a tool and encapsulated according the principal sketch shown in Figure 4.2. Each plate is covered by a release film that does not adhere to the laminate and therefore can be removed easily after cure. The laminate is surrounded by strips of cork making sure that the resin stays in the plate when it becomes more viscous. Next, a breather is placed with purpose to allow air to flow over the entire tool. Around the edges of the tool suction channels are placed, on top of which the valve is connected, to further ease the air flow. Finally a vacuum film is attached to the tool edges.

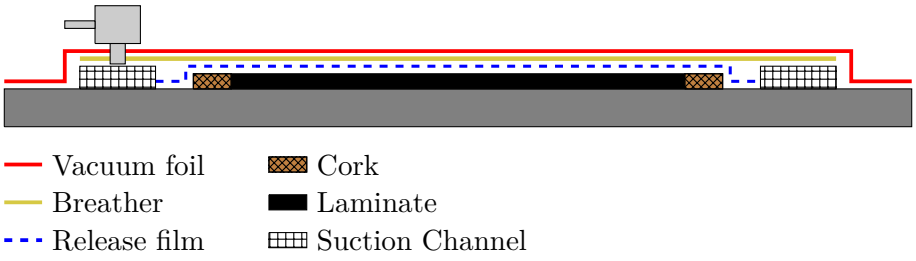

Figure 4.2: Setup for curing in autoclave.

The plates are then cured in an autoclave according to recommendations from Oxeon, illustrated in Figure 4.3. The epoxy system used in the pre-impregnated glass fibre weave has the recommended curing temperature 180 °C which is not reached in the used curing cycle. To circumvent this, a low temperature increase rate of 2 °C/min is used to ensure that the epoxy in the glass fibre weave can fully cure. The slope of the dashed line is unknown as the plates are cooled down unassisted. Before and after the curing, each plate is weighted in order to estimate the fibre volume fraction.

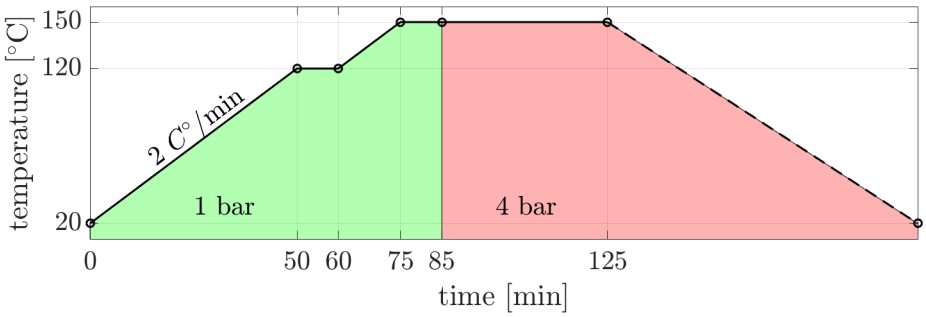

Figure 4.3: Curing cycle recommended by Oxeon for the carbon fibre tape.

From the manufactured plates strips are cut out with with a diamond blade into dimensions presented in the previous section. To these, tabs are fitted on the grip sections to protect the specimen from damage when clamped in the test machine. The tabs are cut out from glass fibre/epoxy plates with thickness 1 mm, the surfaces are roughened with sandpaper and cleaned with ethanol before attached to the specimens with a two component epoxy adhesive with specified shear strength 23.5 MPa. This should give sufficient adhesion according to the guidance from the standard ASTM 3039 [38] that states, given the ultimate tensile strength F^{tu}, coupon thickness t and ultimate shear strength of adhesive F^{su}, that the minimum length

$$L_{min} = \frac{F^{tu}t}{2F^{su}} \approx \frac{2000\,\text{MPa} \cdot 0.48\,\text{mm}}{2 \cdot 23.5\,\text{MPa}} = 20\,\text{mm} \tag{4.3}$$

is enough. That giving a safety factor 2 to the 40 mm used here. After the specimens have been cut out and tabs have been bonded to the grip sections, the look like the one shown in Figure 4.4.

Figure 4.4: A C-specimen with tabs bonded to the grip sections.

4.1.4 Surface treatment

The edges of the test specimens are grinded and polished to avoid premature crack initiation due to stress concentrations at surface imperfections. Polished surfaces are also necessary for the visibility of transverse cracks in an optical microscope where each individual fibre has to be distinguishable. Furthermore, no scratches can be present as they can be mistaken to be cracks. The procedure is carried out by holding the specimen by hand and press the edges gently on a sandpaper attached to a rotating disc, to which finer and finer grits are applied for the grinding. The polishing is carried out similarly but with the use of a lubricant that contains small grains. Three guidelines were discovered during trial and error.

1. For the rough sandpaper with grit size less that 1200-grit, the grit sizes should be decreased in small steps since the material removal is large. Otherwise there is a risk that scratches remain.

2. There is no noticeable gain to use finer sandpapers than with grit size 2400.

3. If the specimen is grinded down with grit size 2400, it is enough to use lubricant with 3 µm grains in the polishing procedure. There is no gain to use the rougher 9 µm before and finer 1 µm afterwards.

Based on the conclusions above, sandpapers with grit sizes 500, 800, 1200 and 2400 are used stepwise for the grinding and 3 µm grains is used for the polishing. For grinding 3 min is used for each step and specimen edge and for polishing 5 min is used per edge. In Figure 4.5 the obtained result of the surface treatment is shown.

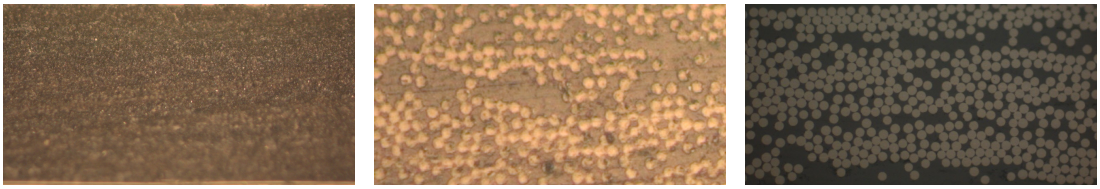

(a) 500-grit **(b)** 2400-grit **(c)** 3 µm

Figure 4.5: Images of the surface quality after three different steps in the surface treatment procedure.

4.1.5 Evaluation of laminate quality

The quality of the laminate is evaluated in terms of fibre volume fraction and void content. The fibre volume fraction, V_f, is calculated based on the weight of fibres and weight of the matrix, W_f and W_m, and the density of the fibre and the matrix, ρ_f and ρ_m, as

$$V_f = \frac{W_f/\rho_f}{W_f/\rho_f + W_m/\rho_m} \tag{4.4}$$

where the weights are obtained from Equation (4.5) as the total weight of the laminate before and after curing is known, as well as the resin content before curing.

$$W_f = (1 - RC\%) \cdot W^{\text{before}}, \quad W_m = W^{\text{after}} - W_f \tag{4.5}$$

After the manufacturing and post-treatment of the test specimen, the void content is measured using the built-in image processing toolbox in Matlab called Color Thresholder, in which individual colours can be thresheld. The mean void content in each laminate can therefore be obtained by taking 20 pictures with location chosen randomly at the edge of some specimens from that laminate and inspect them for black spots, which correspond to voids. The percentage is then averaged over the these 20 images.

4.1.6 Set-up of tensile test machine

The tests are carried out using a tensile test machine located in the Materials and Manufacture lab at Chalmers. It is manufactured by Instron and is equipped with a 50 kN

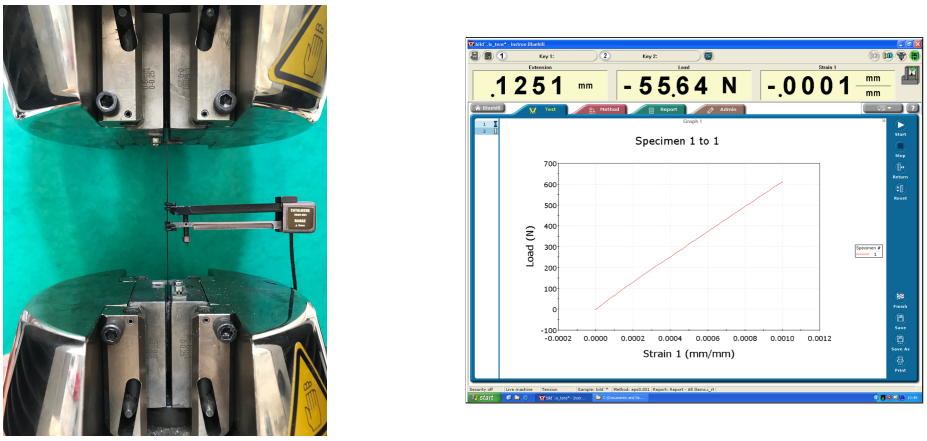

Figure 4.6: Test specimen mounted in the test machine and software BlueHill.

load cell. The test specimen is mounted to the machine using hydraulic grips to which a pressure is applied to the top and bottom grip individually. At this stage, it is important to apply a pressure not too low, which may cause slippage, and not too high, which may damage the test specimen. A study conducted in 2011 by Belingardi et al. [39] showed that 35 bar gave the optimal result, with a final failure in between the grips. The hydraulic pump used is designed for higher pressures up to 1000 bar and is therefore inaccurate for such small as 35 bar making it difficult to be consistent. It could differ as much as ± 10 bar from test to test, which introduces an uncertainty to be considered when analysing the result.

When the test specimen is clamped in the grips an extensometer is mounted symmetrically to the mid-span and mid-width of the specimen. It has two knives at the end that are kept in place by the use of two rubber bands. Information about the strain and load is given continuously to a software called BlueHill in which a strain controlled programme is written that performs the extension at the recommended strain rate of 0.01 min^{-1} [38]. A graph with strain on the x-axis and load on the y-axis is visualised as the programme is running. The set-up is shown in Figure 4.6.

4.1.7 Crack identification

Each specimen is now strained between 0.5-1.5 % with incremental steps of 0.1 %. After each strain increment it is removed from the test rig and put under an optical microscope, called Leica Leitz DMRX, where it is inspected for cracks along the edges. The microscope is equipped with a camera AxioCam MRc5 connected to the software AxioVision. Further, the microscope used has a maximum magnification of 1000x, which is sufficient to inspect individual plies as 20 µm magnifies to 2 cm. To ensure that cracks are not missed due to closure after unloading, the specimen is mounted in a smaller device that allows a smaller tensile load to be applied during the inspection. This device has a 1 kN load cell and the specimen is attached with pins running through holes made through the tabs. It is then loaded with 300 N from recommendations by Dr Loukil, Rise Sicomp. In this case it corresponds to around 0.05 % stain for the C-specimens and around 0.1 % for the G-

specimens. This should be enough to open up potentially closed cracks. The number of cracks is counted on each side of the specimen for each strain level giving data on crack onset and crack density. For the crack to count it must extend through the entire thickness and must not initiate from large voids.

Apart from studying the dependency of stiffness which differs between the C- and G-specimens, an objective with the latter one is to see weather a crack propagates instantaneously over the width or if it grows gradually with increasing strain. This can be done due to the transparency of the glass fibres by, while the specimen is subjected to a load, apply light on one side and photograph the other. The hypothesis is that light will shine through where there are cracks. This is studied for each of the strain levels presented above.

4.2 Finite element analysis

This section presents the methodology for modelling initiation and propagation of a single transverse matrix crack using cohesive zone modelling (CZM). The model is three-dimensional and represents a laminate with three plies, of which the inner-ply is oriented perpendicular to the tensile load. An XFEM crack is used for element splitting. The aim is to predict the tensile in-situ strength of the embedded ply for varying inner-ply thicknesses. Furthermore, the stability of the crack growth is investigated. Firstly, basic concepts of the model is descried followed by the implementation in Abaqus. Finally, a mesh convergence study is conducted.

4.2.1 Model description

A principal sketch of the geometry of the model is shown in Figure 4.7, where the x-axis represents the longitudinal direction and the y-axis represents the transverse direction in a laminate. The model consists of three rectangular geometries blocked together, one for each ply in a $[0/90]_s$-laminate. To reduce the computational cost related to number of elements, symmetry is used about the xy-plane and the xz-plane. The considered geometry is marked in grey in the figure and as a result of the symmetries, the size is reduced to a quarter. As a consequence, only half the real thickness of the 90°-ply is modelled.

At $x = 0$ the surfaces are prohibited to translate in x-direction and at the opposite side a predefined uniform displacement in x-direction is applied to simulate a tensile load. Further, a plane is predefined through the middle rectangle which is highlighted in red in Figure 4.7. This is the cohesive zone where element separation is allowed to initiate and propagate, with aim to mimic the behaviour of a crack. The fracture mechanics theory implies that cracks initiates from local defects in the material where stress concentrations are present. The most realistic approach to model local defects would be to include a statistical distribution of material inhomogeneties. However, Van der Meer and Dávila concluded in 2012, that the same crack characteristic is obtained by inserting a single material defect [33]. Therefore, a small circular defect is inserted at the free edge of the 90°-ply, i.e. at the outer end of the cohesive zone.

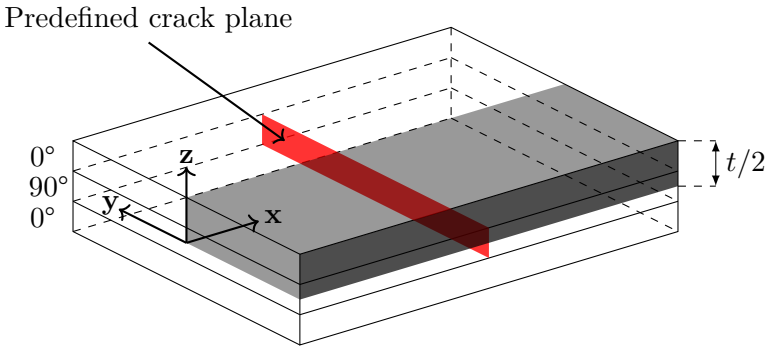

Figure 4.7: Schematic figure of a $[0/90]_s$-laminate. The grey area is the domain after use of symmetry planes and the predefined crack plane highlighted in red.

To capture the damage propagation, a bi-linear traction-separation law for pure Mode I is used. The principle is shown in Figure 3.3 where a linearly elastic response primarily is seen between the separation δ and traction τ. When the interface strength τ^0 is reached at a certain separation δ^0 the element separation initiates, however, there is still traction between the surfaces which degrades linearly until the final separation δ^f. At that point the surfaces are fully separated - corresponding to a crack existing at that specific location. The area below the curve is the critical energy release rate G_{Ic}, i.e. the energy dissipated during fracture per unit of newly created fracture surface area.

In this case the failure criterion is given in terms of the maximum stress. Also defining G_{Ic} then gives the slope of the degradation. A crack is said to be present when the entire cohesive zone is fully degraded and no traction is left between the two surfaces.

4.2.2 Model setup and implementation in Abaqus

The entire analysis is performed in Abaqus/CAE with a static implicit integration scheme. Below, the model implementation and post processing in the software is explained in detail.

Geometry and material parameters

The geometry explained above is created by extruding a rectangle with dimensions $10 \times 10 \times t/2$ mm^3. This is partitioned into two building blocks, one representing the adjacent 0°-ply and one representing half the 90°-ply. The dimensions are not the same as for the test specimens in the experimental study due to the extremely fine mesh required in the end. Furthermore, the thickness of the block that represents the transverse ply is varied between 0.06 mm to 0.4 mm while the adjacent block is fixed at 0.12 mm for all simulations. Homogenised material properties are used for the composite, and the different fibre orientations are represented by assigning the material properties in accordance with the fibre orientations.

Similar to the experimental study, simulations are conducted for two different material configurations, i.e purely in carbon fibre/epoxy and with glass fibre/epoxy for the block

that represents the 0°-ply. All the material parameters can be seen in Table 4.4 where index 1 defines for longitudinal direction and index 2 and 3 the two transverse directions to the fibres. Note that the glass/epoxy is a weave which gives the same elastic modulus in longitudinal and transverse direction.

Material description	E_{11} [GPa]	E_{22} [GPa]	G_{12} [GPa]	ν_{12} [–]	ν_{23} [–]
carbon/epoxy	164	11.5	5.5[a]	0.3[a]	0.4[a]
glass/epoxy	17[b]	17[b]	3[b]	0.15[a]	0.4[a]

[a]Estimated values based on similar materials
[b]From material supplier

Table 4.4: Material properties used in simulations.

Lastly, the damage evolution is defined as a material property where the critical energy release rate, G_{Ic}, and interface strength, τ^0, are specified. In this study, $G_{Ic} = 170\,\mathrm{J/m^2}$ and $G_{Ic} = 220\,\mathrm{J/m^2}$ will be investigated. Together with the elastic properties, a bi-linear traction-separation law can now be created which describes the elastic response and the softening of the material after the interface strength is reached.

Predefined crack plane

The predefined crack plane shown in Figure 4.7 is introduced to the geometry by creating a small plane through the width of the 90°-ply with the thickness of one element. For all the elements within this segment, Abaqus built in XFEM code is applied. This creates an enrichment of the degrees of freedom, described in Section 3.2, that allows elements to split and creates additional nodes at the newly created surfaces. The nodes on the surfaces are allowed to separate, where the separation is determined by the traction-separation law. When there is no traction left in some part of the cohesive zone, crack is said to exist at that location. During the analysis, the growth of the XFEM discontinuity through damaged elements is tracked and once all the elements have fully separated, the matrix crack is assumed fully developed.

To ensure that the separation initiates at the same location for each simulation, a circular defect shown in Figure 4.8 is placed in the middle of the modelled transverse ply. It was observed that the shape and radius of this defect did not affect the crack propagation significantly. Hence, the radius is set to $R_{\mathrm{defect}} = 0.4t_{90}$ in all simulations.

Boundary conditions, mesh and convergence

The symmetry planes explained in Section 4.2.1 are specified by prescribing one translation and two rotations to zero for each plane. The displacement in x-direction is then fixed to zero at $x = 0$ and at the opposite edge a displacement is inserted which is ramped from zero to its maximum value. In Figure 4.9, the placements of the boundary conditions can be seen. Since the theoretical model developed by Dvorak and Laws does not take thermal residual stresses into account, the curing process will not be included in the simulations.

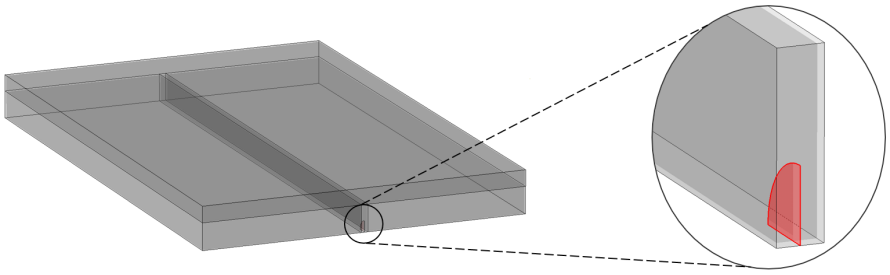

Figure 4.8: Predefined defect with the shape of a quarter-circle used as initiation spot for the XFEM crack.

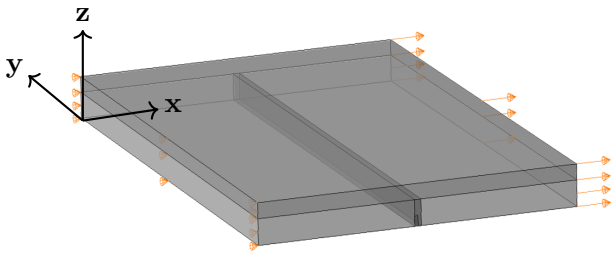

Figure 4.9: Boundary conditions applied on modelled geometry.

Abaqus does not support quadratic elements for XFEM and therefore 8-node linear brick elements, C3D8, are used in the analysis. To save computational cost, reduced integration is used for all elements except for the elements in the predefined crack plane. When doing so, only one integration point in the centroid of the element is used instead of 8 integration points. However, full integration is required for the elements in the crack plane in order to prevent unrealistic hour glass shaped deformations.

Simulations including damage evolution may cause convergence difficulties due to softening of the material model. Hence, a viscous regularisation is used in order to stabilise the response during damage progression and guarantee a positive definite tangent stiffness matrix. For this, a viscous coefficient that is small enough not to influence the results is inserted. Further, to ensure convergence when damage occurs, the displacement has be applied in very small load increments. However, before damage initiation there is no need for such small load increments and an adaptive increment size scheme is used through the simulation.

Output

The in-situ tensile strength is assumed to be reached once the crack begins to propagate. Y_{is}^{T} is extracted from the model by looking at the stress state far away from the crack plane at that time step. Thereafter, a comparison can be made to the theoretical model in Equations (2.5) and (2.7).

Furthermore, the crack propagation is captured for each load increment by monitoring the element separation. From this the stability of the crack is investigated. If the strain has to be increased for the crack to propagate, it is stable. If the crack initiates and propagate through the entire width at the same strain level, it is unstable.

4.2.3 Model calibration and mesh convergence

The interface strength, τ^0, has to be calibrated in order to get a proper crack propagation. If τ^0 is lower than the sought in-situ strength, a uniform degradation of the entire crack plane will occur since τ^0 is reached in all elements. As a result, an unrealistically large plastic zone will be obtained. This can be seen in Figure 4.10 where elements in red are fully degraded, elements in green partially degraded and elements in white non-damaged. The partially degraded elements represents the cohesive or plastic zone. In the left figure, the entire crack plane is partially degraded which indicates that the chosen interface strength is too low. In the right figure however, only the elements in the vicinity of the crack tip is damaged and the crack can grow from one edge to the other. Hence, τ^0 is increased until this behaviour is obtained. The simulated laminate with the thinnest 90°-ply requires the highest interface strength and the corresponding τ^0 value will be used for all simulations.

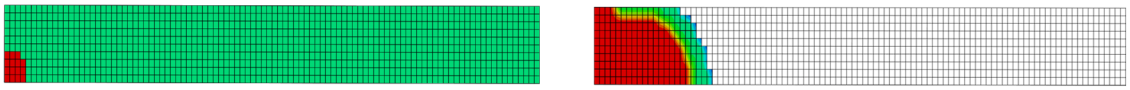

Figure 4.10: Degradation of crack plane with τ^0 lower than the in-situ strength to the left and τ^0 greater than the in-situ strength to the right.

For CZM, as explained in Section 3.3, a certain number of elements across the cohesive zone length, l_{cz}, are required to properly resolve the cohesive zone. By increasing τ^0 the cohesive zone is reduced which requires finer elements along the crack plane. In a previous study by Van der Meer et al. [29] it was found that a mesh size finer than 0.1 mm did not affect the outcome significantly. However, in this study thinner plies will be studied, resulting in a higher interface strength as explained above. A mesh convergence study is therefore conducted for the chosen τ^0. In Figure 4.11 the measured in-situ strength is plotted against number of elements along the crack plane and element length. Three different interface strengths are used, $\tau^0 = 250\,\text{MPa}$, $\tau^0 = 240\,\text{MPa}$ and $\tau^0 = 230\,\text{MPa}$ with a critical energy release rate $G_{Ic} = 220\,\text{J/m}^2$. Convergence is reached with fewer elements as the interface strength is decreased. A small variation can also be seen in the converged values. For consistency, $\tau^0 = 250\,\text{MPa}$ will be used throughout and convergence is reached after 100 elements along the crack plane, which corresponds to an element length $l_e = 0.01\,\text{mm}$.

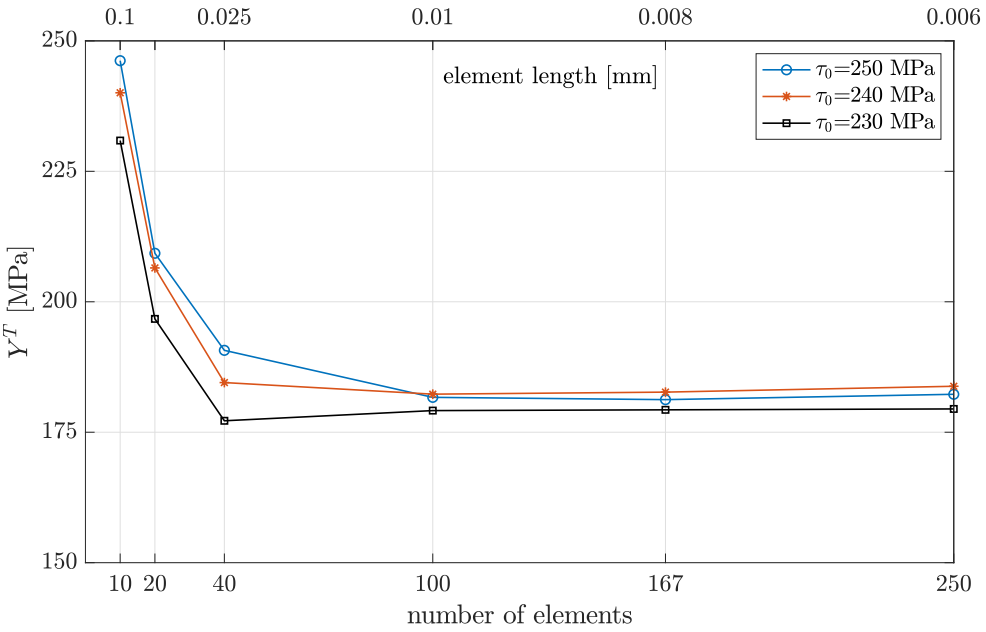

Figure 4.11: Convergence study for three different interface strength values with thickness $t_{90} = 0.2\,\text{mm}$.

5

Results

In this chapter the outcomes from all the parts of the study is presented. It consists of one section for the experimental study and one for the numerical study.

5.1 Experimental analysis

The results from the experiments are shown in this section. Firstly, the outcome from the manufacturing in terms of laminate quality is presented, followed by the result from the tensile testing including onset of transverse cracks and crack density.

5.1.1 Manufacturing outcome

The quality of the laminates manufactured is shown in Table 5.1. The mean thickness of the two C-laminates were 0.61 mm and 0.65 mm respectively, which is 27 % and 35 % more than the expected 0.48 mm. The achieved thickness is therefore around 25.4-27.1 µm compared to the tabulated thickness 20 µm of the tape. The difference in thickness between C240 and C20-120 is partly caused by the difference in void content which affects the thickness. C20-120 has a void content more than twice the value for C240. The fibre volume fraction is 0.7 percentage points larger for C240 than for C20-120.

The G-laminate is 27 % thicker than expected with the tabulated 0.1 mm thickness of the woven E-glass/epoxy fabric, which is around 0.127 mm after manufacturing. The void content in the 90°-layer for the G-specimen is 1 %, which is significantly less than for the C-specimens. The fibre volume fraction is not available for the G-laminates due to missing weight data.

Table 5.1: Fibre volume fraction and void volume fraction for the manufactured laminates.

Laminate	Before [g]	After [g]	Fibre [%]	Void [%]	Thickness [mm]
C20-C120	27.56	27.63	50.18	7	0.65
C240	60.12	59.65	50.87	4	0.61
G20-240	-	-	-	1	1.31/1.33/1.36/1.44/1.57

In Figure 5.1, two representative images of the C20-120 and C240-laminates are shown. A pattern is seen that voids generally occur at the interface between plies, and specifically between plies where there is a change in fibre orientations. As described previously, there is only resin applied on one side of the tape, which results in one potentially drier side of the laminate. Evidence of that was observed as some flaking occurred on that side of the laminate when the specimens were cut and grinded.

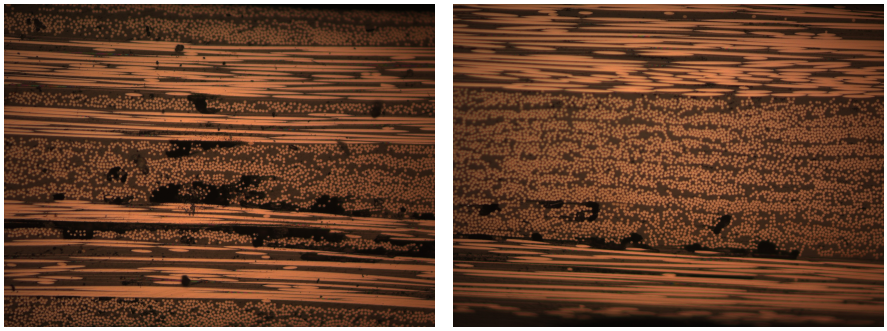

(a) C20-120 **(b)** C240

Figure 5.1: Representative images of specimen quality for C20-120 and C240.

5.1.2 Material properties

From the tensile tests some information of the material properties is obtained. In Figure 5.2 a stress-strain graph from the tensile tests is shown for the G-specimens together with the mean elastic modulus. It is seen that adding more 90°-plies reduces the elastic modulus of the specimen. Therefore the elastic modulus of the woven E-glass/epoxy fabric is around 16.5 GPa, and the transverse elastic modulus for the tape must be below below 13.4 GPa. Concerning the C-specimens, which all have the same elastic modulus theoretically, mean value have been evaluated to 70 GPa, which gives $E_L = 127 - 135$ GPa assuming $E_T = 5 - 13$ GPa.

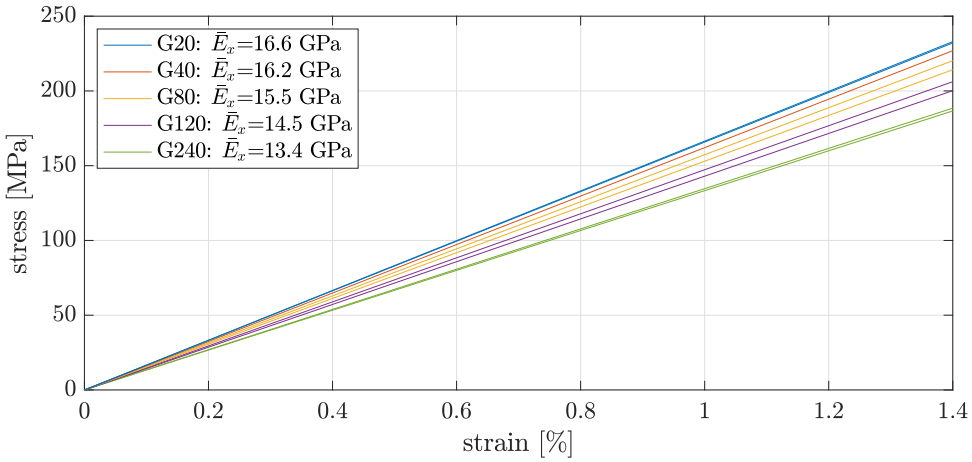

Figure 5.2: Stress-strain relations obtained from tensile testing of the G-specimen.

5.1.3 Identification of transverse cracks

A few specimens for each inner-ply thickness were studied in the microscope with a tensile load 300 N applied using the device described in 4.1.7. This was to investigate whether the cracks close or not when unloading a specimen. In none of the observations did additional cracks appear when the load was applied. A general observation was that for reduced thicknesses the cracks became more difficult to identify, as shown in Figure 5.4. However, applying 300 N in tension did not make any significant difference.

To track the propagation of cracks and to be able to investigate whether the crack grows stably or not, light was applied behind the C-specimens while loaded. This method turned out not to be suitable for C20-C40 as light slipped through even when no cracks were present. For C80-C240 no light came through even when cracks had initiated. In Figure 5.3 examples are shown for C20 and C120. The regularly appearing darker areas in the C20-specimen are interfaces between tapes. As a result, the stability of the crack could not be established from the test results.

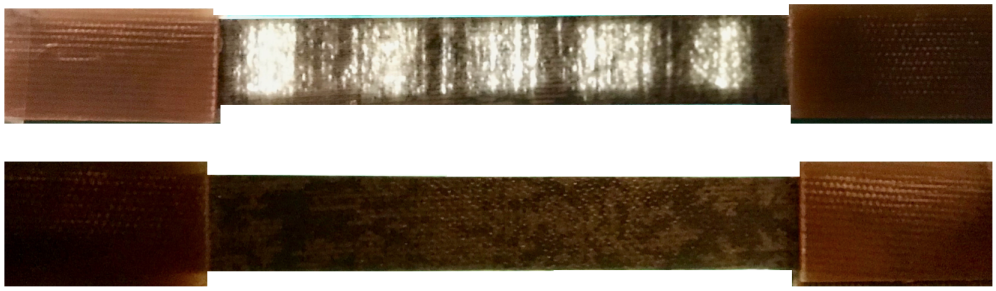

Figure 5.3: Light applied behind a C20- and C120-specimen.

In Figure 5.4 two examples are shown of what matrix cracks looks like in the microscope. The crack in Figure 5.4a is from a G80 specimen and the crack in Figure 5.4b is from a G240 specimen. As can be seen they extend from one end to the other, orthogonal to the adjacent plies, without passing any voids. That is the definition of transverse matrix crack in the continuation of the presentation of results.

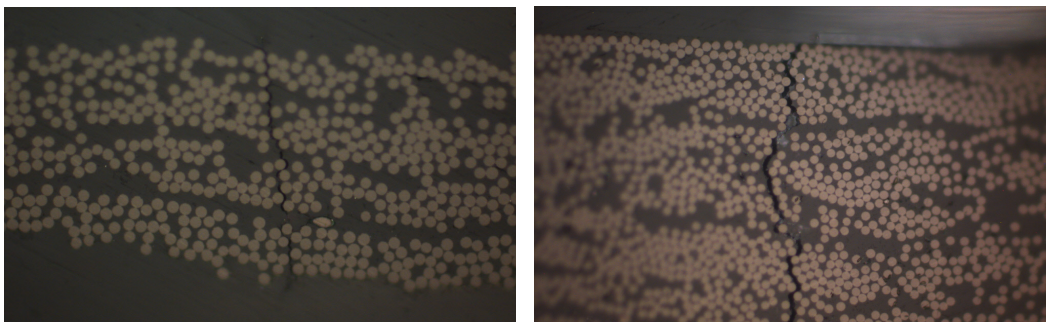

(a) G80 **(b)** G240

Figure 5.4: Identified matrix cracks in G80 and G240 specimen with no load applied during microscopy.

5.1.4 Crack onset

For the C-specimens, the thickness dependency on the onset of transverse cracks is presented to the left in Figure 5.5. Also the analytical model with $G_{Ic} = 220\,\mathrm{J/m^2}$ is plotted to show its correlation to the tests. Final failure occurred at 1.1 %. No cracks appeared prior to final failure for specimens with 90°-plies thinner than 120 µm. It is therefore certain that the strain for onset of transverse cracks increase when decreasing the thickness from 0.12 mm to 0.08 mm, the exact values, however, remain unknown.

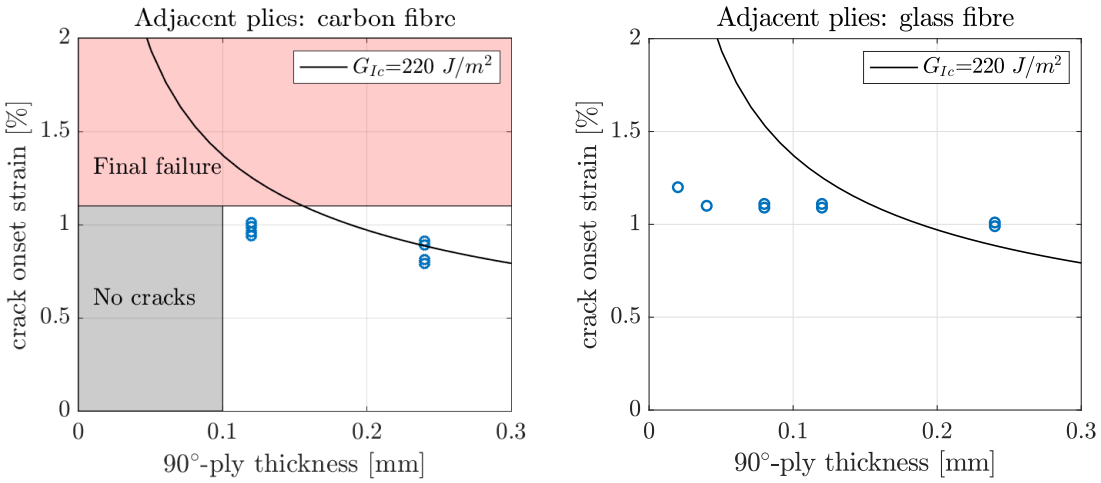

Figure 5.5: Thickness dependency on the onset of transverse cracks for test specimen purely in carbon fibres to the left and with outer-plies in glass fibres to the right.

To the right in Figure 5.5 the onset of transverse crack is shown for the G-specimens. Also here the analytical model with $G_{Ic} = 220\,\mathrm{J/m^2}$ is plotted. In this case the problem with final failure before crack onset did not arise. This is explained by the significantly higher strain to failure of the glass fibre outer-plies compared to the carbon fibre composite. Smaller shear stresses in the interface to the tabs allowed for lower pressure to be applied by the grips, which in turn reduced risk for introducing damage and premature failure. However, the transverse crack onset strain does not increase substantially with decreasing thickness. Regarding the thickness, it is seen that the fibres in inner-ply align with the 90°-tows in the woven glass fibres fabric to create a thicker ply than intended at many locations. An example of this is shown in Figure 5.6, where a 0.02 mm-ply interact with a tow from the glass fibre weave with a combined thickness similar to the conventional 0.12 mm. As a result the transverse crack coincides with the crack in the adjacent GFRP ply.

There is a small difference in the crack onset stain between C and G, where the onset for the G-specimen is shifted slightly higher than for the C-specimen. It is around 0.1 percentage points which could arise due to differences in thermal expansion that introduces stresses during the curing process. A specific E-glass/epoxy composite has the transverse thermal expansion coefficient $\alpha_T = 22.10 \times 10^{-6}\,°\mathrm{C}^{-1}$ which is close to the longitudinal thermal expansion coefficient $\alpha_L = 8.60 \times 10^{-6}\,°\mathrm{C}^{-1}$. For carbon-epoxy composites the thermal coefficients vary multiple orders of magnitude between the longitudinal and transverse direction, for example T300-epoxy have $\alpha_T = 22.5 \times 10^{-6}\,°\mathrm{C}^{-1}$ and $\alpha_L = 0.02 \times 10^{-6}\,°\mathrm{C}^{-1}$

Figure 5.6: Interaction between inner-ply and 90°-tow in glass fibre weave to create thicker inner-ply than intended.

[40] resulting in larger thermal stresses in an embedded 90°-ply than for the E-glass/epoxy. Using classic laminate theory, and the coefficients presented here, the 90°-plies in the C-specimens have the thermal stress 30.5 MPa transversely and the G-specimen have around 12 MPa depending on the thickness of the 90°-ply. A transverse stiffness at 11.5 GPa then gives difference in thermal expansion 0.126-0.145 percentage points which is approximately the offset that was obtained. The difference for each case is shown in Table 5.2.

Table 5.2: The difference in thermal strain between C- and G-specimen for different 90°-ply thicknesses.

90°-ply thickness [mm]	0.02	0.04	0.08	0.12	0.24
$\Delta\varepsilon^T$ [%]	0.126	0.129	0.133	0.136	0.145

5.1.5 Crack density

Due to the premature failure of the C-specimens, no data on the crack density could be obtained. However, for the G-specimens, which did not suffer from that problem, crack density could be measured up to 1.4 %. The results, which are plotted in Figure 5.8, are mean values from the measurements. The trend seen between G240 and G120 is that the crack density decreases with with smaller thickness. However, it is seen that decreasing the thickness further does not do any significant difference, similarly to the tendency seen for the onset of cracks. The cracks appear equidistantly, shown with an example in Figure 5.7, which is expected considering the stress state around cracks. The normal stress is zero at the cracks and then builds up to a peak between two cracks.

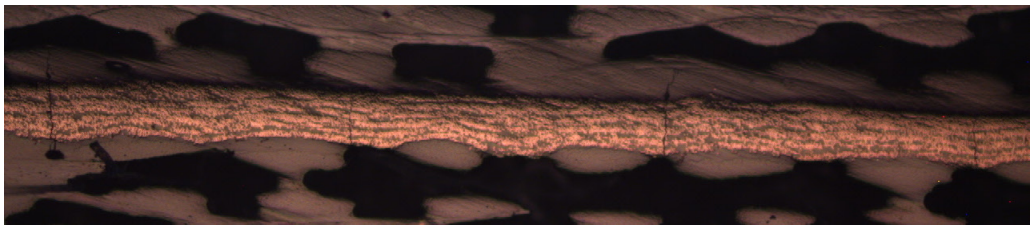

Figure 5.7: Equidistant appearance of cracks in a G120-specimen

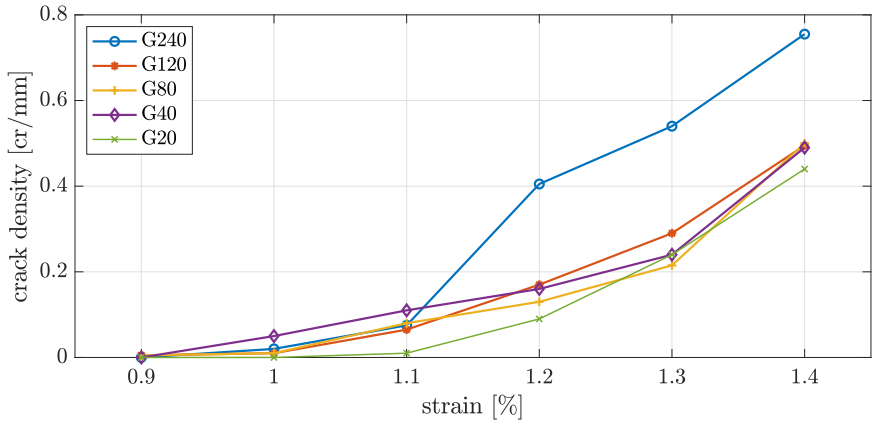

Figure 5.8: Mean value of crack density for test C-specimen.

5.2 Finite element analysis

The outcome from the XFEM cohesive zone model is presented in this section. Firstly, the estimated in-situ tensile strength from the developed model is presented followed by a visualisation of the obtained crack evolution.

5.2.1 Estimated in-situ tensile strength from XFEM model

In all simulations, material parameters in Table 4.4 are used and the element size is set to 0.006 mm which proved to give mesh convergence. Further, the thickness of the block that represent the 90°-ply is varied between 0.06 mm and 0.4 mm. The estimated in-situ tensile strength, Y_{is}^T, from the developed model is shown in Figure 5.9 for simulations of the carbon/epoxy composites. For illustration, two different critical energy release rates have been used, $G_{Ic} = 220\,\mathrm{J/m^2}$ and $G_{Ic} = 170\,\mathrm{J/m^2}$. The dotted lines corresponds to the theoretical models for thick- and thin-plies where $G_{Ic} = 220\,\mathrm{J/m^2}$ is used for the thin-ply theoretical model and $Y^T = 43\,\mathrm{MPa}$ is used for the thick-ply theoretical model. In line with the theoretical models, the in-situ tensile strength is reduced when the critical energy release rate is reduced in the simulations.

The estimated in-situ tensile strength for simulations with glass/epoxy as adjacent plies is shown in Figure 5.10 together with the case with carbon/epoxy for the whole model. Here, the critical energy release rate is set to $G_{Ic} = 220\,\mathrm{J/m^2}$. It can be seen that the two material configurations gives almost the same result for thicknesses above 0.15 mm. For the thinnest regime however, the simulations with glass/epoxy gives a noticeable reduction in in-situ strength.

In Figure 5.11, all the results from the experiments and FE are shown in the same plot together with the analytical model for $G_{Ic} = 220\,\mathrm{J/m^2}$. Large differences can be seen between them. The experiments align relatively well with the analytical for the thicker cases while the FE model correspond better for the thinner cases.

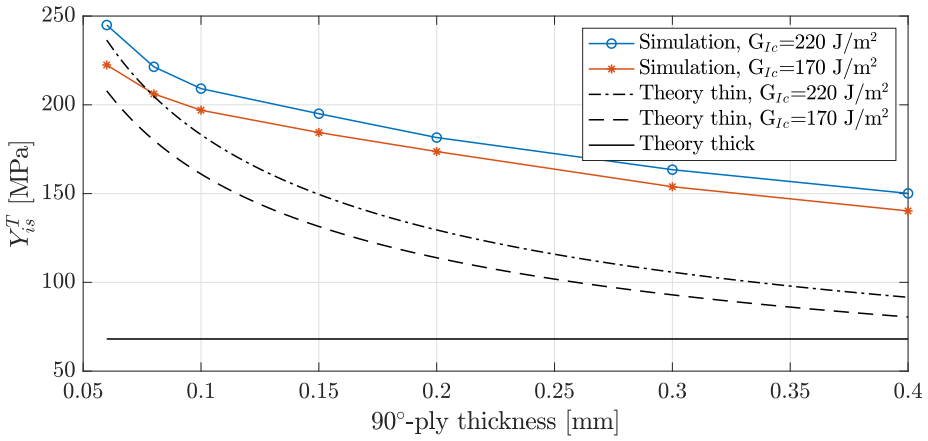

Figure 5.9: Estimated in-situ transverse tensile strength from the developed cohesive zone model compared to the analytical model in Equations (2.5) and (2.7).

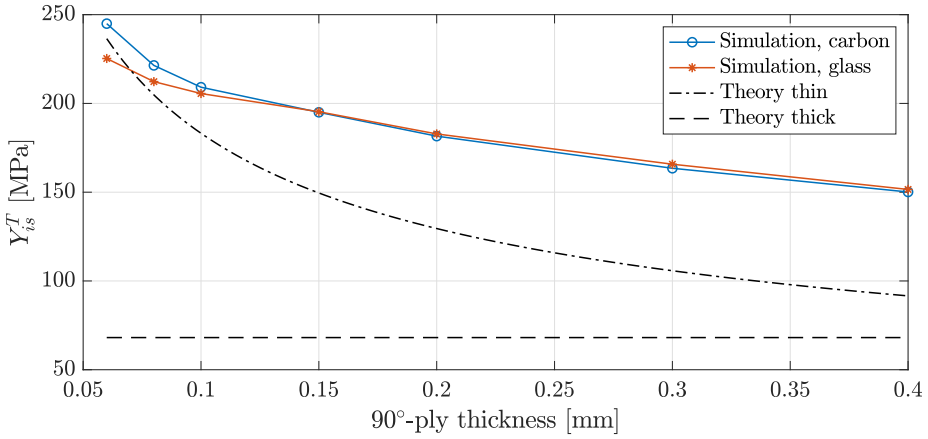

Figure 5.10: Estimated in-situ transverse tensile strength for the two different material configurations.

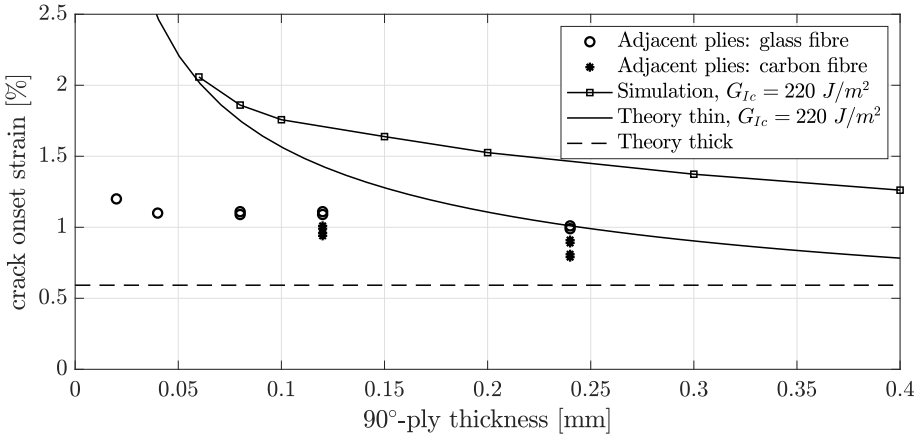

Figure 5.11: All the results from the experimental and numerical analysis plotted together with the analytical model for $G_{Ic} = 220\,\mathrm{J/m^2}$.

5.2.2 Propagation of transverse crack

The obtained crack propagation for $t_{90} = 0.2\,\text{mm}$ and $t_{90} = 0.08\,\text{mm}$ are shown in Figure 5.12 where the cross section of the crack plane is depicted for different strain levels. The material used is carbon/epoxy for the whole model and $G_{Ic} = 220\,\text{J/m}^2$. Note that only half of the transverse ply is presented and that the adjacent 0°-ply is not included. The traction free elements, where a crack is formed, are coloured in red, partially degraded elements are coloured in green and non-damaged elements are in white. Initially, the elements within the predefined defect are traction free. Thereafter, the a cohesive zone is formed around the crack tip, and eventually the separation is large enough to cause the crack to grow. In the interface between the plies, the separation is not large enough to fully split the elements.

For the thick-ply case, once the crack initiates, the propagation is unstable which can be interpreted by the applied strain depicted in the figure. Clearly, the crack propagates without any increase in load. For the simulated thicknesses $t_{90} \leq 0.08\,\text{mm}$ with $G_{Ic} = 220\,\text{J/m}^2$ this is not the case anymore. As can be observed in Figure 5.12, the crack growth is steady to begin with and at a certain point, the crack transforms to an unstable crack propagation. However, it should be noted that the distance of stable crack growth is only 0.2 mm. For all other simulated material configurations, i.e, carbon/epoxy for the whole model with $G_{Ic} = 170\,\text{J/m}^2$ and glass/epoxy as constraining plies with $G_{Ic} = 220\,\text{J/m}^2$, the crack propagation is unstable for all thicknesses.

For the case with glass/epoxy as adjacent plies, the elements near the interface fully degrades as the crack propagates. This holds for all simulated thicknesses and is illustrated in Figure 5.13 for $t_{90} = 0.08\,\text{mm}$.

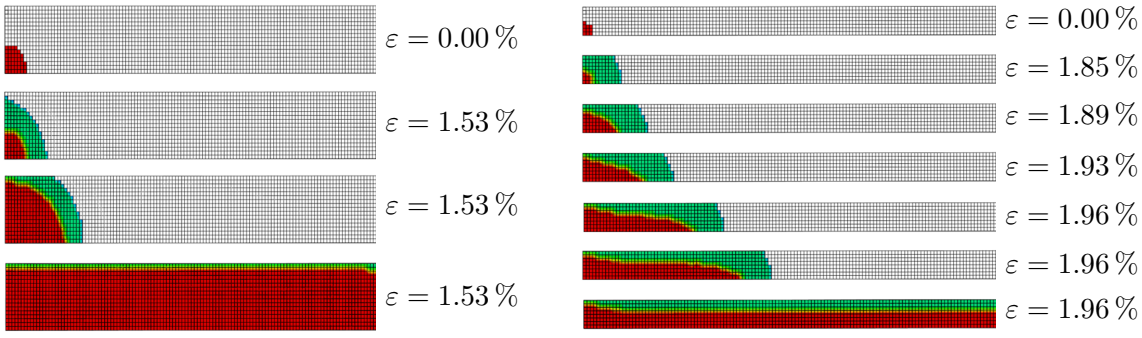

Figure 5.12: Simulated transverse crack propagation with carbon/epoxy for thicknesses $t_{90} = 0.2\,\text{mm}$ to the left and $t_{90} = 0.08\,\text{mm}$ to the right with corresponding applied strain values. Traction free zone (fully degraded) in red, partially degraded zone in green and non-damaged zone in white.

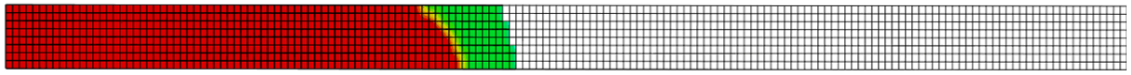

Figure 5.13: Simulated crack propagation with glass/epoxy for the adjacent blocks that represent the 0°-plies.

6

Discussion

This chapter contains a discussion on the results obtained in the study, including possible reasons for the outcome, possible error sources and comparisons to other studies. The chapter is divided into two section, one for the experimental analysis and one for the FE analysis.

6.1 Experimental analysis

From the experimental analysis it can be seen from the C-specimens that the strain for onset of transverse crack was delayed when decreasing the 90°-ply thickness from 0.24 mm to 0.12 mm. It can also be seen that when the thickness is further reduced, crack onset was delayed even more, although the exact strain level remains unknown due to premature final failure. The results correlate quite well to similar studies shown in the Literature Review chapter. For those thicknesses the cracking strain seem to lie around, or just below 1 %, which is also the case for this study.

For the G-specimens almost no increase in onset of cracking strain is observed for decreasing inner-ply thickness, see Figure 5.5. Reasons for this is discussed later on. Focusing instead on the results for the two cases with thickest inner-plies, and comparing them to the corresponding results obtained from the C-specimens, one can note that the measured strain to crack onset differs by approximately 0.1 % unit. One possible explanation for this difference observed is that the difference in stiffness of the adjacent plies have an influence on the in-situ strength. In this case the C-specimens are five times as stiff. However, a more plausible explanation is the effect of thermal residual stresses introduced. These differ between the two cases and correspond well to the difference in crack onset strain. This indicates that the difference in stiffness of the adjacent plies does not have a significant effect on transverse crack formation.

In Figure 5.8 it can be seen that the variation in measured crack density for G20–G120 is very small. This is probably due to the fact that transverse cracks interact with the 90°-tows in the adjacent glass fibre weave, see Figure 5.6. For the thinner inner-plies tested, the thickness contribution from the weave is large compared to the original thickness of the transverse ply. As a result, a thickness dependency of the crack density cannot be established. However, looking at the result for the two thickest inner-plies, it can be seen that the crack density decreases with decreasing thickness. The values that are obtained

coincide with data by yet unpublished experiments conducted by Loukil et al.

The reason for premature final failure in the C-specimen and lack of thickness dependency in the G-specimens, as well as other lessons learned, in terms of manufacturing and the test are discussed below.

6.1.1 Manufacturing

The poor outcome from the manufacturing may have several reasons. Firstly, the resin content 38 %RC in the tape could be too low to wet the entire laminate. Another uncertainty is the curing procedure, where the cycle may not have been conducted according to the recommendations in terms of pressure and temperature. This uncertainty is found as none of the project participants was present at the curing occasion. Even though the curing was conducted according to the recommendations, this cycle may not be optimal either. Concerning the laminates containing both glass fibre weave and carbon fibre tape, which have different recommended curing cycles, it is known that insufficient temperature was reached for the glass fibre fabric. The set-up of the curing is a potential error source if sufficient airflow could not be obtained the way the suction channels and breather films were placed. Patou et. al studied the influence of void content on the mechanical properties and concluded that all strength parameters were reduced when the porosity was increased [41]. Hence, the structural integrity of the manufactured laminates is most likely affected by the high void content present. Optimal for the study would have been to iterate the manufacturing until desired quality could be obtained, however, time was a limiting factor.

As the study primarily has focus related to thickness dependency, using a glass fibre weave turned out not to be optimal. Since glass fibre tows regularly coincide with the 90°-ply, no consistency in thickness could be guaranteed. In fact, data for inner-ply thicknesses below the thickness of a glass fibre tow is not to be considered valid. For future reference a unidirectional glass fibre tape would be preferred to circumvent this issue.

6.1.2 Test

Experimental tests are linked to many sources of error, such as accuracy of instruments. In this case that includes the extensometers, load cells and grip equipment. During testing there were some parts from which more specific lessons could be learned, described here.

To grip the test specimen in the test machine turned out to be a major difficulty. Since the recommended grip pressure for composites is far below the usual working range of the one used in this project, it is impossible to be consistent. A slight increase in pressure leads to failure close to the tab, which is evidence of damage being introduced to the test specimen. It is therefore desirable to decrease the pressure, however, that introduces another problem - slippage and failure in the tab bonding. The two component epoxy adhesive used could not withstand enough shear stress that was introduced if the pressure was decreased in the grip. This balancing act resulted in a premature final failure in the C-specimen at around 1.1 % instead of the tabulated 2.2 %.

To ease the possibility to identify cracks, equipment was used that allows a small load to be applied to the test specimen and doing microscopy simultaneously. It was noted that the crack became more and more difficult to identify as the thickness decreased, however, the recommended 300 N applied did not result in a significant difference. It remains uncertain whether this load is insufficient to open up closed cracks or if it simply is not needed because the cracks actually do not close. An improvement to be considered in the future is to arrange a rig that allows microscopy at the same time that the test specimen is strained. Conclusions in this subject could be drawn more securely with such a rig. This would have other benefits such as saved time related to the mounting and demounting of the test specimen in the test rig. It would also lessen potential damage that arise when pressure is applied and removed to the grip section multiple times.

The human factor plays a major role when cracks are counted. Especially when the quality of the material is such that voids and defects can be mistaken for cracks. If a crack starts from a void, it is hard to know whether it is there as a consequence of a stress concentration from the void or if it would have appeared anyway. It is important to remain consistent throughout the test to find trustworthy trends.

One of the objectives of the study was to find a method that allows crack propagation to be seen as a test specimen is strained. The method proposed was to use the laminate with carbon fibres in the 90°-ply and glass fibre in the adjacent 0°-plies. Due to the transparency of the glass, propagation should be seen when light is applied on one side of a test specimen and photograph the other. However, for specimen with really thin inner plies, there are so few carbon fibres that light shined through everywhere independently of the existence of cracks. For the specimen with thicker inner-plies no light could be seen, which indicate that the cracks in those cases do not let any light through. A development of this method is to improve the light conditions that were not optimal here. The entire test area should be darkened and no light should be able to pass to the side of the test specimen which is photographed, except through the test specimen.

6.2 Finite element analysis

The developed model showed promising results in terms of the ability to predict an in-situ effect in a cross-ply laminate. It also showed, similar to the experimental study, that the difference in elastic properties between glass/epoxy and carbon/epoxy had very little influence on the in-situ strength. However, the numerical model predicts significantly higher in-situ strength then the available theoretical model does. This theoretical model has proven, through previous studies, to correlate well with experimental data and possible error sources and challenges with the FE model will be addressed here.

Furthermore, the model successfully captured the stability/instability of the crack. Previous literature often refer to the intersection between Equations (2.5) and (2.7) as the transition between stable and unstable crack growth which for the used material would be around $t_{90} = 0.7\,\text{mm}$. The results obtained from simulations indicate that this transition occurs at a much smaller thickness. In the simulations, the crack initially grows in a stable manner parallel to the fibres for thicknesses $t_{90} \leq 0.08\,\text{mm}$. When a critical crack length is reached, a transition to unstable growth occurs. In the simulations, the distance of stable

crack growth was found to be very short. Hence, it is of interest to investigate further if the distance covered by stable crack growth is increased for even thinner plies than what was simulated in this study. Experimental studies with the use of computer tomography scan or similar equipment are also necessary for validation.

6.2.1 Simplifications and assumptions

There are a few simplifications made in the model that can potentially influence the result. First of all, the model is based on a single crack. This means that the stress redistribution caused by adjacent cracks is not captured in the model. This is expected to have little influence for the simulated crack onset and crack propagation, but would affect predictions of crack density.

Delamination is not included between the modelled plies. As a result, the adjacent simulated 0°-plies will prevent the crack to open near the interfaces in an unrealistic manner. In reality, delamination would have contributed to crack opening near the interface. This may explain the overestimated in-situ tensile strength and a model with cohesive surfaces between the plies is of interest for future work.

Lastly, the initial size of the defect was chosen to $R_{\text{defect}} = 0.4t_{90}$ which means that the defect scales linearly with the thickness. Even though the crack characteristics did not change when the size of the defect was changed, it should be taken into consideration that the chosen R_{defect} is not based on any established experimental data.

6.2.2 Cohesive zone modelling

In this project XFEM was used to model the cohesive behaviour. The major advantage is the mesh independence in crack propagation simulations, as splitting of elements is allowed. In this particular case however, the mesh is regular and the transverse crack is perfectly aligned with the elements. One could therefore use cohesive zone modelling with a traction-separation law without XFEM and expect a comparable outcome. This would result in a simpler model without the uncertainties of a built-in XFEM code. On the contrary, for more complex geometries with an irregular mesh, the developed XFEM based model would be beneficial.

One of the greatest challenges with a cohesive zone model is the fine element discretisation required to properly resolve the cohesive zone. Even for a simple geometry in pure Mode I loading, this results in a computationally heavy model, especially when a high critical traction is used for the traction-separation law. This was the main reason why the modelled domain had to be decreased. If a similar method would be used to model transverse cracks in a larger geometry, the computation time would quickly become unreasonably long. In this case, a mesh size sufficient for mesh convergence was used for all simulations. However, as can be seen in Figure 4.11, the outcome varied slightly depending on the chosen τ^0. This is an uncertainty that may be the reason why the simulated in-situ strength differentiates from theoretical values. It should be investigated further.

7

Conclusion

The purpose of the study was to investigate the transverse tensile in-situ effect for thin-ply cross-ply composites with both an experimental study and a numerical study. In summary, all the objectives stated in the Introduction chapter were met. However, due to the obstacles that arose during the experimental study it was difficult to compare the experimental results to the FE results.

The experimental study, despite the manufacturing complications, confirmed the presence of an in-situ effect when the thickness of 90°-plies was decreased below the conventional 0.12 mm. Further it was found that the crack density decreases with thinner plies. The stiffness of the adjacent plies did not have a large impact on the in-situ effect, as the obtained difference between the use of glass fibres and carbon fibres in the adjacent plies could be explained by difference in thermal residual stresses. Although the results should be treated with caution, it gives hints of benefits with the new thin-ply composites motivating further development and research in the area.

Concerning the numerical study it is concluded that it is possible to predict in-situ effect without defining such material properties. However, analytical predictions were difficult to mimic due to dependencies on other material parameters such as the critical energy release rate and interface strength in the traction-separation law. It can also be concluded that when modelling very thin composites with a cohesive zone model, an extremely small element size is necessary in order to accurately resolve the cohesive zone. A maximum element size of 0.006 mm was used here, which makes the method unsuitable for larger structures.

Bibliography

[1] J. Fan and J. Njuguna, "An introduction to lightweight composite materials and their use in transport structures," in *Lightweight Composite Structures in Transport*, pp. 3–34, Woodhead Publishing, 2016.

[2] T. Yokozeki, T. Aoki, T. Ogasawara, and T. Ishikawa, "Effects of layup angle and ply thickness on matrix crack interaction in contiguous plies of composite laminates," *Composites Part A: Applied Science and Manufacturing*, vol. 36, no. 9, pp. 1229–1235, 2005.

[3] K. W. Garrett and J. E. Bailey, "Multiple transverse fracture in 90° cross-ply laminates of a glass fibre-reinforced polyester," *Journal of Materials Science*, vol. 12, no. 1, pp. 157–168, 1977.

[4] A. Parvizi and J. E. Bailey, "On multiple transverse cracking in glass fibre-reinforced epoxy cross-ply laminates," *Journal of Materials Science*, vol. 13, no. 10, pp. 2131–2136, 1978.

[5] F. W. Crossman, W. J. Warren, A. S. D. Wang, and G. E. Law, "Initiation and growth of transverse cracks and edge delamination in composite laminates Part 2. Experimental correlation," *Journal of Composite Materials*, vol. 14, no. 1, pp. 88–108, 1980.

[6] L. A. Berglund, J. Varna, and J. Yuan, "Effect of intralaminar toughness on the transverse cracking strain in cross-ply laminates," *Advanced Composite Materials*, vol. 1, no. 3, pp. 225–234, 1991.

[7] T. A. Sebaey, J. Costa, P. Maimí, Y. Batista, N. Blanco, and J. A. Mayugo, "Measurement of the in situ transverse tensile strength of composite plies by means of the real time monitoring of microcracking," *Composites Part B: Engineering*, vol. 65, pp. 40–46, 2014.

[8] I. G. García, J. Justo, A. Simon, and V. Mantič, "Experimental study of the size effect on transverse cracking in cross-ply laminates and comparison with the main theoretical models," *Mechanics of Materials*, vol. 128, pp. 24–37, 2019.

[9] J. M. Berthelot, "Transverse cracking and delamination in cross-ply glass-fiber and carbon-fiber reinforced plastic laminates: Static and fatigue loading Jean-Marie,"

Applied Mechanics Reviews, vol. 56, no. 1, pp. 111–147, 2003.

[10] E. Adolfsson and P. Gudmundson, "Matrix crack initiation and progression in composite laminates subjected to bending and extension," pp. 2020–2058.

[11] H. Saito, H. Takeuchi, and I. Kimpara, "Experimental evaluation of the damage growth restraining in 90° layer of thin-ply CFRP cross-ply laminates," *Advanced Composite Materials*, vol. 21, no. 1, pp. 57–66, 2012.

[12] D. L. Flaggs and M. H. Kural, "Experimental determination of the in situ transverse lamina strength in graphite/epoxy laminates," *Journal of Composite Materials*, vol. 16, no. 2, pp. 103–116, 1982.

[13] F. W. Crossman and A. S. D. Wang, *The dependence of transverse cracking and delamination on ply thickness in graphite/epoxy laminates*, pp. 118–139. s, ASTMSTP 775, K. L. Reifsnider, Ed., American Society for Testing and Materials, 1982.

[14] G. J. Dvorak and N. Laws, "Analysis of progressive matrix cracking In composite laminates II. First ply failure," *Composite Materials*, vol. 21, pp. 309–329, 1987.

[15] A. S. D. Wang, "Fracture mechanics of sublaminate cracks in composite materials," *Composites technology review*, vol. 6, no. 2, pp. 45–62, 1984.

[16] H. Saito, H. Takeuchi, and I. Kimpara, "A study of crack suppression mechanism of thin-ply carbon-fiber-reinforced polymer laminate with mesoscopic numerical simulation," *Journal of Composite Materials*, vol. 48, no. 17, pp. 2085–2096, 2014.

[17] H. M. El-Dessouky and C. A. Lawrence, "Ultra-lightweight carbon fibre/thermoplastic composite material using spread tow technology," *Composites Part B: Engineering*, vol. 50, pp. 91–97, 2013.

[18] S. Sihn, R. Kim, K. Kawabe, and S. Tsai, "Experimental studies of thin-ply laminated composites," *Composites Science and Technology*, vol. 67, no. 6, pp. 996–1008, 2007.

[19] J. Tao and C. T. Sun, "Influence of ply orientation on delamination in composite laminates," *Journal of Composite Materials*, vol. 32, no. 21, pp. 1933–1947, 1998.

[20] M. R. Wisnom, "Size effects in the testing of fibre-composite materials," *Composites Science and Technology*, vol. 59, no. 13, pp. 1937–1957, 1999.

[21] M. R. Wisnom, B. Khan, and S. R. Hallett, "Size effects in unnotched tensile strength of unidirectional and quasi-isotropic carbon/epoxy composites," *Composite Structures*, vol. 84, no. 1, pp. 21–28, 2008.

[22] R. Amacher, J. Cugnoni, J. Botsis, L. Sorensen, W. Smith, and C. Dransfeld, "Thin ply composites: Experimental characterization and modeling of size-effects," *Composites Science and Technology*, vol. 101, pp. 121–132, 2014.

[23] A. Arteiro, G. Catalanotti, J. Xavier, P. Linde, and P. P. Camanho, "Effect of tow

thickness on the structural response of aerospace-grade spread-tow fabrics," *Composite Structures*, vol. 179, pp. 208–223, 2017.

[24] P. P. Camanho, C. G. Dávila, S. T. Pinho, L. Iannucci, and P. Robinson, "Prediction of in situ strengths and matrix cracking in composites under transverse tension and in-plane shear," *Composites Part A: Applied Science and Manufacturing*, vol. 37, no. 2, pp. 165–176, 2006.

[25] F. P. van der Meer, "Mesolevel modeling of failure in composite laminates: Constitutive, kinematic and algorithmic aspects," *Archives of Computational Methods in Engineering*, vol. 19, no. 3, pp. 381–425, 2012.

[26] A. Arteiro, G. Catalanotti, J. Reinoso, P. Linde, and P. P. Camanho, "Simulation of the mechanical response of thin-ply composites: From computational micromechanics to structural analysis," *Archives of Computational Methods in Engineering*, 2018.

[27] P. P. Camanho, P. Maimí, and C. G. Dávila, "Prediction of size effects in notched laminates using continuum damage mechanics," *Composites Science and Technology*, vol. 67, no. 13, pp. 2715–2727, 2007.

[28] X. Li, S. R. Hallett, and M. R. Wisnom, "A finite element based statistical model for progressive tensile fibre failure in composite laminates," *Composites Part B: Engineering*, vol. 45, no. 1, pp. 433–439, 2013.

[29] F. P. van der Meer and C. G. Dávila, "Cohesive modeling of transverse cracking in laminates under in-plane loading with a single layer of elements per ply," *International Journal of Solids and Structures*, vol. 50, no. 20-21, pp. 3308–3318, 2013.

[30] T. Belytschko and T. Black, "Elastic crack growth in finite elements with minimal remeshing," *International Journal for Numerical Methods in Engineering*, vol. 45, no. 5, pp. 601–620, 1999.

[31] N. Moës, J. Dolbow, and T. Belytschko, "A finite element method for crack growth without remeshing," *International Journal for Numerical Methods in Engineering*, vol. 46, no. 1, pp. 131–150, 1999.

[32] Y. Abdelaziz and A. Hamouine, "A survey of the extended finite element," *Computers and Structures*, vol. 86, pp. 1141–1151, 2008.

[33] F. P. van der Meer and C. G. Dávila, "Modeling transverse cracking in laminates with a single layer of elements per ply," *ECCM-15TH European Conference on composite materials*, 2012.

[34] M. S. Loukil, *Experimental and numerical studies of intralaminar cracking in high performance composites*. PhD thesis, Luleå University of Technology, 2013.

[35] P. P. Camanho, C. G. Davila, and M. F. de Moura, "Numerical Simulation of Mixed-Mode Progressive Delamination in Composite Materials Damage and Failure of Non-

Conventional Composite Laminates View project," *Journal of Composite Materials*, vol. 37, no. 16, pp. 1415–1438, 2003.

[36] A. Turon, P. P. Camanho, J. Costa, and C. G. Dávila, "A damage model for the simulation of delamination in advanced composites under variable-mode loading," *Mechanics of Materials*, vol. 38, no. 11, pp. 1072–1089, 2006.

[37] "Mitsubishi Pyrofil™ MR 70 12P." `https://www.900gpa.com/en/product/fiber/CF_007236E6BE?u=metric&q=m`. Accessed: 2019-05-15.

[38] ASTM D3039/D3039M-17, "Standard Test Method for Tensile Properties of Polymer Matrix Composite Materials," tech. rep., ASTM International, West Conshohocken, PA, 2017.

[39] G. Belingardi, D. S. Paolino, and E. G. Koricho, "Investigation of influence of tab types on tensile strength of E-glass/epoxy fiber reinforced composite materials," *Procedia Engineering*, vol. 10, pp. 3279–3284, 2011.

[40] B. D. Agarwal, L. J. Broutman, and K. Chandrashekhara, *Analysis and performance of fiber composites*. New Dehli: John Wiley & Sons, third ed., 2006.

[41] J. Patou, E. De Luycker, and G. Bernhart, "Influence of void content on the mechanical properties of carbon/PPS laminates," *17th European Conference on Composite Materials*, no. June, pp. 26–30, 2016.